# Widely Separated MIMO Radar Using Matrix Completion

Shunqiao Sun, *Senior Member, IEEE*, Yunqiao Hu, *Student Member, IEEE*, Kumar Vijay Mishra, *Senior Member, IEEE*, and Athina P. Petropulu, *Fellow, IEEE*

***Abstract*— We present a low-complexity widely separated multiple-input-multiple-output (WS-MIMO) radar that samples the signals at each of its multiple receivers at reduced rates. We process the low-rate samples of all transmit-receive chains at each receiver as data matrices. We demonstrate that each of these matrices is low rank as long as the target moves slowly within a coherent processing interval. We leverage matrix completion (MC) to recover the missing samples of each receiver signal matrix at the common fusion center. Subsequently, we estimate the targets' positions and Doppler velocities via the maximum likelihood method. Our MC-based WS-MIMO (MC-WS-MIMO) approach recovers missing samples and thereafter target parameters at reduced rates without discretization of the parameter space. Our analysis using ambiguity functions shows that antenna geometry affects the performance of MC-WS-MIMO. Numerical experiments demonstrate reasonably accurate target localization at SNR of 20 dB and sampling rate reduction to 20%.**

***Index Terms*— Ambiguity function, low-rank data, matrix completion, target localization, widely separated MIMO radar.**

## I. Introduction

DURING the past decade, there has been extensive research interest in multiple-input-multiple-output (MIMO) radars that employ several transmit (Tx) and receive (Rx) antennas [1], [2], [3], [4]. MIMO radars are usually classified as *colocated* or *widely separated* depending on the antenna placement relative to the targets. In a colocated MIMO (CL-MIMO) radar [3], [5], the antennas are placed close enough to observe coherent signals reflected from a target whose radar cross-section (RCS) appears identical to all Tx-Rx antenna pairs. Unlike phased array radar that transmits a single waveform, CL-MIMO transmits multiple mutually orthogonal signals. The waveform diversity can be exploited to achieve high angular resolution [6], [7], and high-quality parameter identifiability [8]. In widely separated MIMO (WS-MIMO) radar, the distance between any two antennas is much larger than their distance from the target, resulting in each Tx-Rx antenna pair seeing a different RCS of the target.

In this paper, we focus on WS-MIMO systems. The spatial diversity in WS-MIMO is advantageous in detecting targets with small backscatter and low speed [9], [10]. The angular diversity provides WS-MIMO a better probability of detection; however, this comes at a cost of increased minimum required signal-to-noise ratio (SNR), below which a phased array radar shows better detection performance [11]. In particular, WS-MIMO exhibits superior detection of Swerling chi-squared target models I and III, that are statistically independent from scan-to-scan, than the CL-MIMO [12]. In an electronic warfare scenario, a WS-MIMO is capable of maintaining the same detection threshold as a monostatic radar but with a lower total radiated power. This decreases the probability of intercepting the radar's transmit signal by hostile entities [13].

WS-MIMO radars are similar to traditional multi-static radars in the sense that they both employ widely separated Tx-Rx units, but they differ from multi-static radar in the way they make a decision about the target. Multi-static radar perform a significant amount of local processing at each receiver, and they use a central unit to fuse the decisions of the local units. WS-MIMO radar jointly processes the signals from all the receivers and makes a single decision about the target. This joint processing approach is beneficial in detecting a spatially diverse target that requires probing from different directions [9], [14], or a *stealth* target [15]. In the latter case, when the target becomes unobservable for specific Tx-Rx pairs, it may escape detection altogether in a multi-static radar because of local processing at each receiver [16].

Even though a WS-MIMO radar provides superior detection over the conventional multi-static network, the use of multiple waveforms in MIMO systems implies the need for several Tx-Rx radio-frequency (RF) chains, resulting in huge hardware costs, high energy consumption, and very large computational complexity [17], [18]. Further, the joint processing of all receivers requires the transmission of the measurements of each antenna to the fusion center, thus involving an additional communications cost. Lately, various techniques have been proposed to address the problem of reducing the cost of hardware, energy, and area in conventional MIMO radars (see, e.g., [19] for a review). These methods exploit the fact that the target scene is *sparse*, and the radar processing tasks can

Manuscript received 29 August 2023; revised 16 December 2023; accepted 28 January 2024. Date of publication 5 February 2024; date of current version 13 February 2024. This work was supported in part by the U.S. National Science Foundation (NSF) under Grant CCF-2153386 and Grant ECCS-2033433. An earlier version of this paper was presented at the 2019 IEEE Radar Conference [DOI: 10.1109/RADAR.2019.8835745]. *(Corresponding author: Shunqiao Sun.)*

Shunqiao Sun and Yunqiao Hu are with the Department of Electrical and Computer Engineering, The University of Alabama, Tuscaloosa, AL 35487 USA (e-mail: shunqiao.sun@ua.edu; yhu62@crimson.ua.edu).

Kumar Vijay Mishra is with the United States DEVCOM Army Research Laboratory, Adelphi, MD 20783 USA (e-mail: kvm@ieee.org).

Athina P. Petropulu is with the Department of Electrical and Computer Engineering, Rutgers, The State University of New Jersey, Piscataway, NJ 08854 USA (e-mail: athinap@rutgers.edu).

Digital Object Identifier 10.1109/TRS.2024.3362693

be modeled as finding sparse solutions to under-determined linear equations - an aspect addressed by the emerging field of compressed sensing (CS) [20].

There is a large body of literature on CS-based CL-MIMO radars that focuses on processing with a reduced number of signal samples, which is common when using fewer RF chains. In [21], a theoretical framework for the recoverability of targets in the azimuth–range and azimuth–range–Doppler domains via sparse approximation algorithms has been proposed for a MIMO radar. In [22], the optimal CS measurement matrix is designed for colocated MIMO radar by considering coherence of the sensing matrix and signal-to-interference ratio as optimality criteria. The approach in [23] combines step frequency with CS in a MIMO radar system to enable high-resolution range, angle, and Doppler estimation with narrowband pulses.

In comparison, relatively fewer studies have examined CS applications to WS-MIMO. The earliest application of CS to recover direction-of-arrival (DOA) with sub-Nyquist samples in a WS-MIMO was formulated in [24]. This was later extended to recovering both position and Doppler velocity of the targets by reducing only the temporal sampling rate in [25], [26], and [27]. In [25], CS is used to accurately estimate the position and velocity of multiple targets in a WS-MIMO radar. A decoupled approach proposed in [26] efficiently handles sparse target returns and reduces computational complexity. Here, the basis matrix columns are reordered to introduce group sparsity. Then, the target estimation problem is formulated as a sparse signal recovery task with magnitude constraints on reflection coefficients, and an ADMM-based solution is proposed to significantly reduce computational complexity and enhance accuracy; performance guarantees for recovery were provided in [28]. A few other studies have exploited sparsity in WS-MIMO toward power allocation [29], [30], optimal detectors [31], dictionary learning [32], and stationary target imaging [33]. In nearly all of these works, the targets are assumed to be located on an angle-Doppler-range grid. In practice, target parameters are typically continuous values the discretization of which may introduce gridding errors [34].

To avoid the off-grid errors while also maintaining high resolution, reduced-rate sampling, and low complexity, predominantly two approaches have been proposed. The first technique [35] formulates the radar parameter estimation for off-grid targets using atomic norm minimization [36] and applies to a CL-MIMO radar. In the second approach, the signal samples received from an array radar are processed as data matrices, which, under certain conditions, are low rank. Then, random temporal sampling at each receiver results in a partially observed data matrix and the missing entries are retrieved using *matrix completion* (MC) methods, which have been extensively studied [37], [38], [39]. State-of-the-art in [37] solves matrix completion problem by minimizing nuclear norm and demonstrates that the missing data is perfectly recovered from limited observations. In [38], matrix completion is extended to the noisy case. Theoretical guarantees in [39] show that the original signal data should follow the strong incoherence property.

Once the matrix is recovered, conventional methods are employed for target parameter recovery and estimation. The MC-based sampling and recovery was first suggested for volumetric targets in a phased-array weather radar [40] and later for point targets in a CL-MIMO radar [41], [42], [43], [44]. In addition to avoiding the grid issue, the MC approach restores the SNR loss because of subsampling. In particular, [43] provided recovery guarantees for MC-based CL-MIMO (MC-CL-MIMO) while corresponding sampling strategies and waveforms were analyzed in [42].

In this paper, we propose off-grid target recovery using MC for a WS-MIMO. The different formulation of this problem, as compared to the CL-MIMO problem makes the extension of prior work to this scenario non-trivial. In MC-CL-MIMO [42], the low-rank data matrix is formulated by samples from all Tx-Rx chains for a single pulse. In MC-based WS-MIMO (MC-WS-MIMO), we exploit the low-rank structure of a matrix formed by samples of a single Tx-Rx chain for all pulses.

Preliminary results of this work appeared in our conference publication [1], which presented initial simulation results for the target localization using the maximum likelihood (ML) approach. In this paper, we also analyze the coherence of the WS-MIMO data matrix that guarantees recovery with MC, investigate the WS-MIMO radar ambiguity function (AF), derive the Cramér-Rao lower bound (CRLB) of WS-MIMO radar localization, and provide more comprehensive numerical studies with comparisons to the geometry-based approach. We show that target parameters can be estimated with reasonable accuracy at 20 dB SNR even when the sampling rate is reduced by 20%. Hence, MC offers notable advantages in improving the accuracy of target localization and velocity estimation, particularly in scenarios with low signal-to-noise ratios and reduced sampling rates. Additionally, the MC-based ML estimation exhibits robustness in target localization in these settings. Furthermore, the analysis of AF indicates that the distribution of antennas in WS-MIMO radar impacts the MC-based recovery. In our study, circularly-placed antennas are found to have improved localization than other geometries.

The rest of the paper is organized as follows. In the next section, we introduce the system model of WS-MIMO radar in the context of the MC problem. Section IV-A provides theoretical guarantees for the coherence and recoverability of the data matrix. In Section III, we present the method for estimating the target parameters such as location and velocity. We provide the AF and lower error bounds for our system in Section IV. We validate our methods through numerical experiments in Section V and conclude in Section VI.

Throughout this paper, we reserve boldface lowercase, boldface uppercase, and calligraphic letters for vectors, matrices, and index sets, respectively. The $i$-th element of a vector $\mathbf{y}$ is $y(i)$; the $(i, j)$-th entry of a matrix $\mathbf{Y}$ is $[\mathbf{Y}]_{i,j}$; the $i$-th column of matrix $\mathbf{Y}$ is $\mathbf{y}_i$; and the $i$-th row of matrix $\mathbf{Y}$ is $\mathbf{Y}^{(i)}$. The set of $N$-dimensional vectors of complex numbers is $\mathbb{C}^N$. We use $\mathbf{I}_N$ for the identity matrix of size $N \times N$. We denote the transpose, Hermitian, conjugate transpose, modulus and floor operations by $(\cdot)^T$, $(\cdot)^H$, $(\cdot)^\dagger$, $||\cdot||$, and $\lfloor . \rfloor$,

respectively. The Hadamard (point-wise) and inner products are denoted by $\odot$ and $\langle\cdot,\cdot\rangle$, respectively. The notations $\|\cdot\|_*$ and $\|\cdot\|_{\mathcal{F}}$ are reserved for the nuclear and Frobenius norms of the matrix, respectively. The function $\max(\cdot)$ returns the maximum value of its argument. The cardinality of the set is given by $|\cdot|$.

## II. System Model

We introduce the system model of WS-MIMO radar and show that the data matrix at each receive antenna has a low-rank structure. We then propose a reduced-rate sampling scheme at each receive antenna to obtain partially observed matrices on which we apply MC technique at a fusion center.

### A. WS-MIMO Radar

Consider a WS-MIMO radar system with $M_t$ transmit and $M_r$ receive antennas, located in a two-dimensional (2)-D) Cartesian coordinate system. We denote the position vectors of the $m$-th transmit and $n$-th receive antennas by $\mathbf{p}_t^{(m)} = \left[x_t^{(m)}, y_t^{(m)}\right]^T$ and $\mathbf{p}_r^{(n)} = \left[x_r^{(n)}, y_r^{(n)}\right]^T$, respectively. The waveform orthogonality in WS-MIMO radar is achieved through either time, code, or frequency division multiplexing (TDM, CDM, or FDM) [45]. In this paper, we employ CDM to achieve waveform orthogonality. Each transmit antenna emits a narrowband phase-coded pulse, composed of $N$ subpulses, during each pulse repetition interval (PRI), $T_{\text{PRI}}$; its reciprocal is the pulse repetition frequency (PRF). The baseband waveform of the $m$-th antenna is [46]

$$s_m(t) = \frac{1}{\sqrt{T_p}} \sum_{n=1}^{N} x_m(n)\, p\left[\frac{t-(n-1)t_b}{t_b}\right], \quad m = 1, \cdots, M_t, \tag{1}$$

where $x_m(n) = e^{j\phi_m(n)}, m = 1, \cdots, M_t, n = 1, \cdots, N$ is the phase code, and $p(t)$ is the rectangular subpulse shaping function with amplitude 1 for duration from 0 to 1. Here, $t_b$ is subpulse duration, and $T_p = Nt_b$ is the pulse duration. The orthogonality implies $\int_{T_p} s_i(t) s_j^*(t) dt = \delta(i-j),\ \forall i, j$, where $\delta(\cdot)$ is the Dirac delta function. The transmit waveforms are narrowband such that

$$\frac{\lambda}{c} \ll \frac{1}{B}, \tag{2}$$

where $\lambda = c/f_c$ is the operating wavelength of $m$-th transmitter, $f_c$ is carrier frequency, $c = 3 \times 10^8$ m/s is the speed of light, and $B$ is the bandwidth of WS-MIMO radar system. Each transmitter sends out a pulse train consisting of $Q$ uniformly spaced known pulses $s_m(t)$:

$$s_{m,Q}(t) = \sum_{q=0}^{Q-1} s_m(t - qT_{\text{PRI}}), \quad 0 \le t \le QT_{\text{PRI}}. \tag{3}$$

The duration of all $Q$ pulses is known as the coherent processing interval (CPI).

Assume that the radar target scene consists of $K$ targets distributed in an area denoted by a set of coordinates $\mathcal{S}$, sharing the same 2-D plane as the WS-MIMO transmitters and receivers. The $k$-th target is represented by its gravity center [8] whose position vector is denoted as $\mathbf{p}^{(k)} = \left[x_k, y_k\right]^T$ moving at a velocity of $\boldsymbol{v}^{(k)} = \left[v_x^{(k)}, v_y^{(k)}\right]^T$. The transmit signal is reflected back by the targets and these echoes are collected by each receive antenna. For a given spatially diverse $k$-th target and $m$-th-Tx-and-$n$-th-Rx pair, the radar processor aims to retrieve following information from the received signals: reflection coefficient $\beta_{mn}^{(k)}$, wherein we assumed that the target follows the Swerling I model [47] so that its reflectivity is constant during the CPI; time delay $\tau_{mn}^{(k)}$, which is linearly proportional to the target's location $\mathbf{p}^{(\mathbf{k})}$ as

$$\tau_{mn}^{(k)} = \frac{\left\|\mathbf{p}^{(k)} - \mathbf{p}_t^{(m)}\right\| + \left\|\mathbf{p}^{(k)} - \mathbf{p}_r^{(n)}\right\|}{c}, \tag{4}$$

and Doppler frequency $f_{mn}^k$, which is proportional to the target's radial velocity $\boldsymbol{v}^{(k)}$ as

$$f_{mn}^{(k)} = \frac{f_c}{c}\left(\frac{\left\langle \boldsymbol{v}^{(k)}, \mathbf{p}^{(k)} - \mathbf{p}_t^{(m)}\right\rangle}{\left\|\mathbf{p}^{(k)} - \mathbf{p}_t^{(m)}\right\|} + \frac{\left\langle \boldsymbol{v}^{(k)}, \mathbf{p}^{(k)} - \mathbf{p}_r^{(n)}\right\rangle}{\left\|\mathbf{p}^{(k)} - \mathbf{p}_r^{(n)}\right\|}\right). \tag{5}$$

### B. Operating Conditions

We make the following assumptions on the radar operation and target parameters:

**C1** "Unambiguous time-frequency region": The target locations are assumed to lie in the unambiguous region of delay-Doppler plane $[0, R_{\max}] \times [0, v_{\max}]$, where $R_{\max} = \frac{cT_{\text{PRI}}}{2}$ is the maximum unambiguous range and $v_{\max} = \frac{c}{f_0 T_{\text{PRI}}}$ is the maximum unambiguous velocity in both x- and y-directions, i.e. the time delays are no longer than the PRI and Doppler frequencies are up to the PRF.

**C2** "Low acceleration": The frequency modulation because of a slow-moving target manifests as a frequency shift in the received signal. The targets are slow-moving and have low acceleration so that their time delays and Doppler frequencies are assumed constant over a CPI:

$$\frac{2v_i^{(k)} QT_{\text{PRI}}}{c} \ll \frac{1}{B}, \quad i = x, y, \tag{6}$$

$$f_{mn}^{(k)} T_p \ll 1. \tag{7}$$

**C3** "Constant delays": The Doppler shifts induced are small over a CPI under the condition **C2** so that the delay is approximated to be constant. This allows for the piecewise-constant approximation: $f_{mn}^{(k)} t \approx f_{mn}^{(k)} qT_{\text{PRI}}$, for $t \in [qT_{\text{PRI}}, (q+1))T_{\text{PRI}}]$.

**C4** "Constant Doppler shifts": The velocity change of a target over a CPI is small compared with the velocity resolution such that $\frac{dv_{(\cdot)}^{(k)}}{dt} \ll \frac{c}{2f_0(QT_{\text{PRI}})^2}$, where the subscript $(\cdot)$ denotes either x- or y-directions.

**C5** "Constant reflectivities": The radar-to-target distance is large compared with the displacement of the target during a CPI, allowing the attenuation to be considered constant over a CPI.

**C6** "Unimodular waveforms": Due to practical hardware limitations such as amplifiers and analog-to-digital converters, the waveforms need to be unimodular, that is, they must maintain a constant modulus.

### C. Receive Data Matrix With Low Rank Structure

The received signal at the $n$-th receive antenna is

$$y_n(t) = \sum_{q=0}^{Q-1}\sum_{m=1}^{M_t}\sum_{k=1}^{K}\sqrt{E}\beta_{mn}^{(k)}s_m\left(t-\tau_{mn}^{(k)}-qT_{\mathrm{PRI}}\right) \times e^{\mathrm{j}2\pi\left(f_c+f_{mn}^{(k)}\right)\left(t-\tau_{mn}^{(k)}\right)}+w_n(t), \quad (8)$$

where $w_n(t)$ is the additive spatio-temporally white, zero mean Gaussian noise with variance $\sigma_n^2$, and $\sqrt{E}$ is waveform energy. After demodulation and passing the baseband signal through an anti-aliasing low-pass filter, the received signal at the $n$-th receiver for the $m$-th carrier frequency is

$$y_{mn}(t) = \sum_{q=0}^{Q-1}\sum_{k=1}^{K}\sqrt{E}\beta_{mn}^{(k)}s_m\left(t-\tau_{mn}^{(k)}-qT_{\mathrm{PRI}}\right) \times e^{\mathrm{j}2\pi f_{mn}^{(k)}t}e^{-j2\pi\left(f_c+f_{mn}^{(k)}\right)\tau_{mn}^{(k)}}+w_{mn}(t). \quad (9)$$

For the sake of simplicity, the term $e^{-j2\pi\left(f_c+f_{mn}^{(k)}\right)\tau_{mn}^{(k)}}$ can be absorbed into the target reflection coefficient $\beta_{mn}^{(k)}$. Hence, the baseband received signal at the $n$-th receive antenna and transmitted from the $m$-th transmit antenna is

$$y_{mn}(t) = \sum_{q=0}^{Q-1}\sum_{k=1}^{K}\sqrt{E}\beta_{mn}^{(k)}s_m\left(t-\tau_{mn}^{(k)}-qT_{\mathrm{PRI}}\right)e^{\mathrm{j}2\pi f_{mn}^{(k)}t}+w_{mn}(t), \quad (10)$$

where $w_{mn}(t)$ is the noise term.

We denote the maximum and minimum ranges of all possible target locations in the coordinate set $\mathcal{S}$ with respect to the $m$-th transmit and $n$-th receive antennas as $R_{mn}^{(\max)}$ and $R_{mn}^{(\min)}$, respectively. Denote the Nyquist sampling interval by $T_s$ so that $N$ samples of the pulse duration ($T_p = NT_s$) are obtained. For each pulse received, we set the sampling window length at each receive antenna as $N+L_{mn}^{(\max)}$ to collect unambiguous samples for every possible location in an area covered by $\mathcal{S}$, where $L_{mn}^{(\max)} = \left\lfloor \frac{R_{mn}^{(\max)}-R_{mn}^{(\min)}}{cT_s} \right\rfloor$. Define $L_{mn}^{(k)} = \left\lfloor \frac{R_{mn}^{(k)}-R_{mn}^{(\min)}}{cT_s} \right\rfloor$, where $R_{mn}^{(k)} = c\tau_{mn}^{(k)}$ is the distance corresponding to the total time of flight from the $m$-th transmitter to the $k$-th target and back from the same target to the $n$-th receiver.

Define $\mathbf{C}_{L_{mn}^{(k)}} = \left[\mathbf{0}_{N\times L_{mn}^{(k)}}\ \mathbf{I}_N\ \mathbf{0}_{N\times\left(L_{mn}^{(\max)}-L_{mn}^{(k)}\right)}\right] \in \mathbb{C}^{N\times\left(N+L_{mn}^{(\max)}\right)}$. The Nyquist samples from each of the $N+L_{mn}^{(\max)}$ range-cells for the $q$-th pulse are collected in the following vector

$$\mathbf{y}_{mn}^{(q)} = \mathbf{z}_{mn}^{(q)} + \mathbf{w}_{mn}^{(q)},\ q = 0,\cdots,Q-1, \quad (11)$$

where $\mathbf{w}_{mn}^{(q)}$ is the sampled noise vector and the signal trail is

$$\mathbf{z}_{mn}^{(q)} = \sum_{k=1}^{K}\sqrt{E}\beta_{mn}^{(k)}(q)e^{\mathrm{j}2\pi f_{mn}^{(k)}qT_{\mathrm{PRI}}}\mathbf{C}_{L_{mn}^{(k)}}^{T}\mathbf{s}_m = \mathbf{A}_{mn}\mathbf{x}_{mn}^{(q)}, \quad (12)$$

where $\mathbf{A}_{mn} = \left[C_{L_{mn}^{(1)}}^{T}\mathbf{s}_m,\cdots,C_{L_{mn}^{(K)}}^{T}\mathbf{s}_m\right] \in \mathbb{C}^{\left(N+L_{mn}^{\max}\right)\times K}$ and $\mathbf{x}_{mn}^{(q)} = \left[\beta_{mn}^{(1)}e^{\mathrm{j}2\pi f_{mn}^{(1)}qT_{\mathrm{PRI}}},\cdots,\beta_{mn}^{(K)}e^{\mathrm{j}2\pi f_{mn}^{(K)}qT_{\mathrm{PRI}}}\right]^T$.

Here, $\mathbf{s}_m \in \mathbb{C}^{N\times 1}$ is the sampled transmit waveform from the $m$-th transmit antenna. In the above, we used $e^{\mathrm{j}2\pi f_{mn}^{(k)}t} \approx e^{\mathrm{j}2\pi f_{mn}^{(k)}qT_{\mathrm{PRI}}}$ which follows from the condition **C3**.

After collecting samples for $Q$ pulses, we formulate the noise-free signal trail of the data matrix at the $n$-th receiver as

$$\mathbf{Z}_{mn} = \left[\mathbf{z}_{mn}^{(1)},\mathbf{z}_{mn}^{(2)},\cdots,\mathbf{z}_{mn}^{(Q)}\right]^T = \mathbf{D}_{mn}\mathbf{\Lambda}_{mn}\mathbf{\Gamma}_{mn}, \quad (13)$$

where the transmit signal matrix $\mathbf{\Gamma}_{mn} = \left[\mathbf{C}_{L_{mn}^{(1)}}^{T}\mathbf{s}_m\ \cdots\ \mathbf{C}_{L_{mn}^{(K)}}^{T}\mathbf{s}_m\right]^T$, the Doppler matrix $\mathbf{D}_{mn} = \left[\mathbf{d}_{mn}^{(1)},\cdots,\mathbf{d}_{mn}^{(K)}\right]$ and the reflectivity matrix $\mathbf{\Lambda}_{mn} = \mathrm{diag}\left\{\left[\beta_{mn}^{(1)},\cdots,\beta_{mn}^{(K)}\right]\right\}$. Here, $\mathbf{d}_{mn}^{(k)}$ is the Doppler steering vector defined as [48]

$$\mathbf{d}_{mn}^{(k)} = \left[1, e^{\mathrm{j}2\pi f_{mn}^{(k)}T_{\mathrm{PRI}}},\cdots,e^{\mathrm{j}2\pi f_{mn}^{(k)}(Q-1)T_{\mathrm{PRI}}}\right]^T. \quad (14)$$

We have the following result regarding the rank of the noise-free data matrix $\mathbf{Z}_{mn}$.

*Proposition 1: and $\mathbf{Z}_{mn} \in \mathbb{C}^{Q\times\left(N+L_{mn}^{(\max)}\right)}$ be the data matrix formulated from the samples at the n-th receive antenna for the reflected echoes corresponding to the m-th transmit signal. Then, the rank of $\mathbf{Z}_{mn}$ is determined by the number of different ranges as well as different velocities among all targets and the rank is bounded by $K$.*

*Proof:* The matrices $\Gamma_{mn}$ and $\mathbf{D}_{mn}$ in (13) have the dimensions $K\times\left(N+L_{mn}^{(\max)}\right)$ and $Q\times K$, respectively. Under the assumption of slow moving targets, each target stays in the same range bin during a CPI. We note that the rank of matrix $\mathbf{D}_{mn}$ is governed by the velocity differences among all $K$ targets. If more than one targets have the same velocity, the rank of matrix $\mathbf{D}_{mn}$ could be less than $K$. For matrix $\Gamma_{mn}$, its rank is governed by the time-differences-of-arrival $L_{mn}^{(K)}, k = 1,\cdots,K$, which, in turn, are determined by the range differences of all $K$ targets. If more than one targets occupy the same range bin, the rank of $\Gamma_{mn}$ could be less than $K$. Therefore, following (13), the data matrix $\mathbf{Z}_{mn} \in \mathbb{C}^{Q\times\left(N+L_{mn}^{(\max)}\right)}$ is low rank and its rank is bounded by $K$. ■

Combining the noise-trail with $\mathbf{Z}_{mn}$, we obtain the full data matrix

$$\mathbf{Y}_{mn} = \mathbf{Z}_{mn} + \mathbf{W}_{mn}, \quad (15)$$

where $\mathbf{W}_{mn}$ is the sampled noise matrix.

### D. Reduced-Rate Sampling and Matrix Completion

In our MC-WS-MIMO, each receiver samples the incoming signal during each pulse at sub-Nyquist rates. There are several ways to implement a sub-Nyquist sampler [19]. Here, we assume that the samples are selected uniformly at random. For each Tx-Rx pair, these low-rate samples are modeled as partially observed data matrices $\mathbf{X}_{mn} \in \mathbb{C}^{Q\times\left(N+L_{mn}^{(\max)}\right)}$:

$$[\mathbf{X}_{mn}]_{ij} = \begin{cases}[\mathbf{Y}_{mn}]_{ij}, & (i,j)\in\Omega,\\ 0, & \text{otherwise},\end{cases} \quad (16)$$

where $\Omega$ is the set of indices of observed entries with $|\Omega| = h$. The above sampling process can be compactly represented by using the operator $\mathcal{P}_\Omega$ such that $\mathbf{X}_{mn} = \mathcal{P}_\Omega(\mathbf{Y}_{mn})$.

The receiver then forwards these partially observed data matrices to a fusion center which recovers the missing entries by applying MC techniques as follows. From Proposition 1, each of the matrices $\mathbf{Z}_{mn}$, $n = 1, \cdots, M_r$, $m = 1, \cdots, M_t$, is low rank; their rank being bounded by $K$. In the noise-free case, these matrices can be completed by solving the following optimization [37], [39]

$$\begin{aligned} &\text{minimize} \quad \|\mathbf{X}_{mn}\|_* \\ &\text{subject to} \quad \mathcal{P}_\Omega(\mathbf{X}_{mn}) = \mathcal{P}_\Omega(\mathbf{Z}_{mn}), \end{aligned} \tag{17}$$

where the nuclear norm $\|\mathbf{X}_{mn}\|_*$ is the sum of singular values of matrix $\mathbf{X}_{mn}$.

Here, the conditions of MC are related to the bounds on the coherence of $\mathbf{Z}_{mn}$. Assume the compact singular value decomposition (SVD) of $\mathbf{Z}_{mn}$ is $\mathbf{Z}_{mn} = \sum_{k=1}^{K} \rho_k \mathbf{u}_k \mathbf{v}_k^H$, where $\rho_k$, $k = 1, \cdots, K$ are the singular values, and $\mathbf{u}_k$ ($\mathbf{v}_k$) are the corresponding left (right) singular vectors. The subspaces spanned by $\mathbf{u}_k$ and $\mathbf{v}_k$ are $U$ and $V$, respectively. Denote $n_1 = Q$ and $n_2 = N + L_{mn}^{(\max)}$. The coherence of $U$ (and similarly for $V$) is [37]

$$\mu(U) = \frac{n_1}{K} \max_{1 \le i \le n_1} \left\| \mathbf{U}^{(i)} \right\|^2 \in \left[1, \frac{n_1}{K}\right], \tag{18}$$

where $\mathbf{U}^{(i)}$ is the $i$-th row of matrix $\mathbf{U} = [\mathbf{u}_1, \cdots, \mathbf{u}_K]$. The matrix $\mathbf{Z}_{mn}$ has coherence with parameters $\mu_0$ and $\mu_1$ if **A0** $\max(\mu(U), \mu(V)) \le \mu_0$ for some positive $\mu_0$.

**A1** The maximum element of matrix $\sum_{1 \le i \le K} \mathbf{u}_i \mathbf{v}_i^H$ is bounded by $\mu_1 \sqrt{K/(n_1 n_2)}$ in absolute value for some positive $\mu_1$.

If the matrix $\mathbf{Z}_{mn}$ satisfies **A0** and **A1**, the following theorem provides a probabilistic bound for the number of observed entries needed to successfully recover matrix $\mathbf{Z}_{mn}$.

*Theorem 1 [37]: Suppose we observe $h$ entries of a rank-$K$ matrix of $\mathbf{Z}_{mn} \in \mathbb{C}^{n_1 \times n_2}$ uniformly at random. Assume $b = \max(n_1, n_2)$. There exist constants $C$ and $\zeta$ that if*

$$h \ge C \max\left(\mu_1^2, \mu_0^{1/2}\mu_1, \mu_0 b^{1/4}\right) \gamma K b \log b, \tag{19}$$

*for some $\gamma > 2$, the minimizer to problem (17) is unique and equal to $\mathbf{Z}_{mn}$ with probability of $1 - \zeta b^{-\gamma}$. For $K \le \mu_0^{-1} b^{1/5}$, the bound can be improved to $m \ge C \mu_0 b^{6/5} \gamma K \log b$, without affecting the probability of success.*

In the presence of noise, we have $\mathcal{P}_\Omega(\mathbf{Y}_{mn}) = \mathcal{P}_\Omega(\mathbf{Z}_{mn}) + \mathcal{P}_\Omega(\mathbf{W}_{mn})$. Then, $\mathbf{Z}_{mn}$ is completed by solving the optimization

$$\begin{aligned} &\text{minimize} \quad \|\mathbf{X}_{mn}\|_* \\ &\text{subject to} \quad \|\mathcal{P}_\Omega(\mathbf{X}_{mn} - \mathbf{Y}_{mn})\|_\mathcal{F} \le \delta, \end{aligned} \tag{20}$$

where $\delta^2 = \left(h + \sqrt{8h}\right)\sigma^2$ and $\sigma^2$ is the covariance of noise. Denote he solution to the optimization problem (20) by $\hat{Z}_{mn}$. Then, the error norm is bounded as $\left\|\hat{Z}_{mn} - \mathbf{Z}_{mn}\right\|_\mathcal{F} \le 4\sqrt{(2n_1n_2 + m)\min(n_1, n_2)/m}\delta + 2\delta$ [38]. The common singular value thresholding (SVT) algorithm [49] can be applied to solve the above nuclear norm problem.

## III. Target Localization

Once the matrices $\mathbf{Z}_{mn}, m = 1, \cdots, M_t, n = 1, \cdots, M_r$ are recovered via MC technique at the fusion center, the unknown target parameters are estimated using any of the classical signal processing techniques such as ML [50], least squares, or sparse reconstruction methods [25]. Since the target parameters in a WS-MIMO are usually statistically modeled, we adopt the ML approach for target localization here.

### A. Maximum Likelihood Method

Denote the unknown target parameters by $\boldsymbol{\theta} = \left[x, y\right]^T \in \Theta$, where $\Theta$ is a two-dimensional space that includes all possible values of $(x, y)$. Assume the hypotheses $\mathcal{H}_1$ and $\mathcal{H}_0$ correspond to, respectively, the presence and absence of the target return in the received signal in (11) that follows the distribution

$$\mathbf{y}_{mn}^{(q)} \sim \mathcal{N}_C\left(\mathbf{z}_{mn}^{(q)}, \sigma_n^2 \mathbf{I}\right), \tag{21}$$

where $\mathcal{N}_C$ denotes the complex multivariate circularly symmetric Gaussian probability density function. The negative log-likelihood ratio (LLR) of hypotheses $H_1$ and $H_0$, is

$$\mathcal{L}_{mn}(\boldsymbol{\theta}, \mathbf{Y}_{mn}) = \frac{1}{\sigma_n^2} \sum_{q=0}^{Q-1} \left\| \mathbf{y}_{mn}^{(q)} - \mathbf{A}_{mn} \mathbf{x}_{mn}^{(q)} \right\|^2. \tag{22}$$

Since the noise and target reflection coefficients are statistically independent, the joint likelihood ratio is the product of individual likelihood ratios. The joint negative LLR is

$$\begin{aligned} \mathcal{L}(\boldsymbol{\theta}) &= \sum_{m=1}^{M_t} \sum_{n=1}^{M_r} \mathcal{L}_{mn}(\boldsymbol{\theta}, \mathbf{Y}_{mn}) \\ &= \sum_{m=1}^{M_t} \sum_{n=1}^{M_r} \sum_{q=0}^{Q-1} \frac{1}{\sigma_n^2} \left\| \mathbf{y}_{mn}^{(q)} - \mathbf{A}_{mn} \mathbf{x}_{mn}^{(q)} \right\|^2. \end{aligned} \tag{23}$$

By minimizing (23) over $\mathbf{x}_{mn}^{(q)}$, the least squares solution is

$$\hat{\mathbf{x}}_{mn}^{(q)} = \mathbf{A}_{mn}\left(\mathbf{A}_{mn}^H \mathbf{A}_{mn}\right)^{-1} \mathbf{A}_{mn}^H \mathbf{y}_{mn}^{(q)}. \tag{24}$$

By substituting (24) in (23), the joint negative LLR function becomes

$$\mathcal{L}(\boldsymbol{\theta}) = \sum_{m=1}^{M_t} \sum_{n=1}^{M_r} \sum_{q=0}^{Q-1} \frac{1}{\sigma_n^2} \left\| \mathbf{P}_{mn}^{\perp} \mathbf{y}_{mn}^{(q)} \right\|^2, \tag{25}$$

where $\mathbf{P}_{mn}^{\perp} = \mathbf{I} - \mathbf{A}_{mn}\left(\mathbf{A}_{mn}^H \mathbf{A}_{mn}\right)^{-1} \mathbf{A}_{mn}^H$ is the orthogonal projection matrix on the column space of $\mathbf{A}_{mn}$. The ML estimate of the parameter vector $\boldsymbol{\theta}$ is

$$\hat{\boldsymbol{\theta}}_{\text{ML}} = \arg\max_{\Theta} \left( - \sum_{m=1}^{M_t} \sum_{n=1}^{M_r} \sum_{q=0}^{Q-1} \frac{1}{\sigma_n^2} \left\| \mathbf{P}_{mn}^{\perp} \mathbf{y}_{mn}^{(q)} \right\|^2 \right). \tag{26}$$

In general, the computationally demanding problem in (26) is solved by nonlinear optimization algorithms such as genetic algorithms and simulated annealing [51]. In this paper, we adopt a two-dimensional search over $\Theta$ to find the peaks of $-\mathcal{L}(\boldsymbol{\theta})$.

### B. Geometric Method

Alternatively, a geometric approach may be employed for localization [52] to obtain a closed-form solution that leads to a reduced computational complexity when compared with the ML approach. For example, [52] employs a two-stage weighted least squares (WLS) to determine the location of a target based on the bistatic range measurements in a passive MIMO radar. Similar closed-form localization algorithms have been suggested for distributed MIMO radars, wherein the transmitters and receivers may or may not be co-located [53]. These approaches require time delay (TD) estimation to get an initial measurement of the range from transmitters to receivers.

Assume that the unknown target position is $\mathbf{p}^{(m)} = \left[x_t^{(m)}, y_t^{(m)}\right]^T$, the $i$-th transmitter placed at known position $\mathbf{p}_t^{(i)} = \left[x_{T_i}, y_{T_i}\right]^{\mathrm{T}}$ for $i = 1, 2, \ldots, M_t$, and the $j$-th receiver at known positions $\mathbf{p}_r^{(j)} = \left[x_{R_j}, y_{R_j}\right]^{\mathrm{T}}$ for $j = 1, 2, \ldots, M_r$. The distance between the target and the $i$-th transmitter is

$$R_{tT_i} = \sqrt{\left(x_{T_i} - x_t\right)^2 + \left(y_{T_i} - y_t\right)^2}. \tag{27}$$

The distance between the target and the $j$-th receiver is

$$R_{tR_j} = \sqrt{\left(x_{R_j} - x_t\right)^2 + \left(y_{R_j} - y_t\right)^2}. \tag{28}$$

Then, the total range $R_{tT_iR_j}$ is

$$\begin{aligned} R_{tT_iR_j} &= R_{tT_i} + R_{tR_j} \\ &= \sqrt{\left(x_{T_i} - x_t\right)^2 + \left(y_{T_i} - y_t\right)^2} \qquad (29) \\ &\quad + \sqrt{\left(x_{R_j} - x_t\right)^2 + \left(y_{R_j} - y_t\right)^2}. \qquad (30) \end{aligned}$$

Reformulate (30) as

$$\begin{aligned} R_{tT_iR_j} - \sqrt{\left(x_{T_i} - x_t\right)^2 + \left(y_{T_i} - y_t\right)^2} \\ = \sqrt{\left(x_{R_j} - x_t\right)^2 + \left(y_{R_j} - y_t\right)^2}. \end{aligned} \tag{31}$$

Squaring both sides of (31), rearranging the terms, and simplifying yields

$$\begin{aligned} \left(x_{R_j} - x_{T_i}\right)x_t + \left(y_{R_j} - y_{T_i}\right)y_t - R_{tT_iR_j}R_{tT_i} \\ = \frac{1}{2}\left(R_{R_j}^2 - R_{tT_iR_j}^2 - R_{T_i}^2\right), \end{aligned} \tag{32}$$

where $R_{R_j}$ ($R_{tT_iR_j}$) are the position coordinates of transmitter (receiver):

$$R_{T_i} = \sqrt{x_{T_i}^2 + y_{T_i}^2}, \tag{33}$$

and

$$R_{R_j} = \sqrt{x_{R_j}^2 + y_{R_j}^2}, \tag{34}$$

Arranging equation (32) in a matrix form with $M_t$ transmitters and $M_r$ receivers leads to the following system of linear equations:

$$\mathbf{A}\mathbf{x} = \mathbf{b}, \tag{35}$$

where

$$\mathbf{A} = \begin{bmatrix} \mathbf{D}_1 & -\mathbf{r}_{t1} & \cdots & \mathbf{0} \\ \mathbf{D}_2 & \mathbf{0} & \cdots & \mathbf{0} \\ \vdots & \vdots & \ddots & \vdots \\ \mathbf{D}_{M_t} & \mathbf{0} & \cdots & -\mathbf{r}_{tM_t} \end{bmatrix} \in \mathbb{C}^{(M_t \times M_r)\times(M_t+3)}, \tag{36}$$

$$\mathbf{x} = \begin{bmatrix} x_t & y_t & R_{tT_1} & \cdots & R_{tT_{M_t}} \end{bmatrix}^{\mathrm{T}}, \tag{37}$$

$$\mathbf{b} = \begin{bmatrix} \mathbf{b}_1^{\mathrm{T}} & \mathbf{b}_2^{\mathrm{T}} & \mathbf{b}_3^{\mathrm{T}} & \cdots & \mathbf{b}_{M_t}^{\mathrm{T}} \end{bmatrix}^{\mathrm{T}}, \tag{38}$$

$$\mathbf{D}_i = \begin{bmatrix} x_{R_1} - x_{T_i} & y_{R_1} - y_{T_i} \\ x_{R_2} - x_{T_i} & y_{R_2} - y_{T_i} \\ \vdots & \vdots \\ x_{R_{M_r}} - x_{T_i} & y_{R_{M_r}} - y_{T_i} \end{bmatrix} \in \mathbb{C}^{M_r \times 2}, \tag{39}$$

$$\mathbf{b}_i = \frac{1}{2}\begin{bmatrix} R_{R_1}^2 - R_{tT_iR_1}^2 - R_{T_i}^2 \\ \vdots \\ R_{R_{M_r}}^2 - R_{tT_iR_{M_r}}^2 - R_{T_i}^2 \end{bmatrix} \in \mathbb{R}^{M_r \times 1},\ i = 1, \cdots, M_t, \tag{40}$$

and $\mathbf{r}_{ti} = \left[R_{tT_iR_1}, \ldots, R_{tT_iR_{M_r}}\right]^{\mathrm{T}}$ is the range measurement vector corresponding to the $i$-th transmit antenna, and $\mathbf{r}_t = \left[\mathbf{r}_{t1}, \ldots, \mathbf{r}_{tM_t}\right]^{\mathrm{T}}$ is the range measurement vector for all transmit antennas. Applying the ML method to TD estimation produces [54]

$$\hat{\boldsymbol{\tau}} = \underset{\boldsymbol{\tau}}{\operatorname{argmax}} \frac{\left|\sum_{m=1}^{M_t}\sum_{n=1}^{M_r}\frac{e^{\mathrm{j}2\pi f_c \tau_{mn}}}{\tau_{mn}^{\beta}}\sum_{q=0}^{Q}\mathbf{y}_{mn}^{(q)}\mathbf{s}_{mn}^{\dagger(q)}\right|^2}{\sum_{m=1}^{M_t}\sum_{n=1}^{M_r}\frac{1}{\tau_{mn}^{2\beta}}}, \tag{41}$$

where $\mathbf{y}_{mn}$ is the signal vector transmitted from the $m$-th transmit antenna and received by the $n$-th receive antenna, $\mathbf{s}_m^{\dagger}$ is conjugate transposition of transmit waveform vector of $\mathbf{s}_m$ transmitted from the $m$-th transmit antenna, $\beta$ is path loss. After obtaining the TD estimates, applying WLS yields

$$\hat{\mathbf{x}}_{\text{init}} = \left(\hat{\mathbf{A}}^{\mathrm{T}}\hat{\mathbf{A}}\right)^{-1}\hat{\mathbf{A}}^{\mathrm{T}}\mathbf{b}, \tag{42}$$

from which we obtain the initial target position $\left[\hat{x}_t, \hat{y}_t\right]^{\mathrm{T}}$ as

$$\begin{bmatrix} \hat{x}_t \\ \hat{y}_t \end{bmatrix} = \begin{bmatrix} 1 & 0 & 0 & 0 & \ldots & 0 \\ 0 & 1 & 0 & 0 & \ldots & 0 \end{bmatrix}\hat{\mathbf{x}}_{\text{init}}. \tag{43}$$

The distance between the target and transmitters used for designing the weighting matrix is then computed using $\left[\hat{x}_t, \hat{y}_t\right]^{\mathrm{T}}$. The weighting matrix $\mathbf{W}$ becomes

$$\mathbf{W} = \mathbf{C}_{\boldsymbol{\varepsilon}}^{-1} = ((\boldsymbol{\Lambda} - \boldsymbol{\Gamma})\mathbf{C}_{\boldsymbol{n}}(\boldsymbol{\Lambda} - \boldsymbol{\Gamma}))^{-1}, \tag{44}$$

where $\boldsymbol{\Lambda} = \operatorname{diag}(\mathbf{r}_{\mathrm{t}})$, $\boldsymbol{\Gamma} = \left(\left[R_{tT_1}\mathbf{1}^{\mathrm{T}}, \ldots, R_{tT_{M_t}}\mathbf{1}^{\mathrm{T}}\right]^{\mathrm{T}}\right)$, and $\mathbf{1}$ is a vector of all ones of length $M_r$. The target location estimate is

$$\hat{\mathbf{x}}_{\text{final}} = \left(\hat{\mathbf{A}}^{\mathrm{T}}\mathbf{W}\hat{\mathbf{A}}\right)^{-1}\hat{\mathbf{A}}^{\mathrm{T}}\mathbf{W}\mathbf{b}. \tag{45}$$

### C. Lower Error Bounds

Define the target parameter vector $\boldsymbol{\theta} = [\hat{x}_t, \hat{y}_t, \hat{\xi}_{re}, \hat{\xi}_{im}]$, where $\hat{\xi}_{re}$ ($\hat{\xi}_{im}$) is the real (and imaginary) part of target's complex reflectivity, that needs to be estimated. The CRLB for estimating $\boldsymbol{\theta}$ is [55]

$$\mathbf{CRLB} = \mathbf{J}^{-1}(\boldsymbol{\theta}), \tag{46}$$

where the Fisher information matrix (FIM) is

$$\mathbf{J}(\boldsymbol{\theta}) = E_{\mathbf{y}|\boldsymbol{\theta}}\left\{\left[\frac{\partial}{\partial\boldsymbol{\theta}}\log p(\mathbf{y}\mid\boldsymbol{\theta})\right]\left[\frac{\partial}{\partial\boldsymbol{\theta}}\log p(\mathbf{y}\mid\boldsymbol{\theta})\right]^{\mathrm{T}}\right\}, \tag{47}$$

where $\log p(\mathbf{y}\mid\boldsymbol{\theta})$ is the probability density function (pdf) of received signal $\mathbf{y}$ conditioned on $\boldsymbol{\theta}$ and $E_{\mathbf{y}|\boldsymbol{\theta}}\{\cdot\}$ is the conditional expectation of $\mathbf{y}$ given $\boldsymbol{\theta}$. We are interested in only the target position and, thus, need to extract the $2\times 2$ submatrix of CRLB matrix, i.e., $[\mathbf{CRLB}]_{2\times 2} = \left[\mathbf{J}^{-1}(\boldsymbol{\theta})\right]_{2\times 2}$. Using the Schur complement of block matrix [56],

$$[\mathbf{CRLB}]_{2\times 2} = \left(\mathbf{H}\boldsymbol{\Lambda}\mathbf{H}^{\mathrm{T}} - \mathbf{V}\mathbf{H}\boldsymbol{\Lambda}_{\zeta}^{\mathrm{T}}\mathbf{H}^{\mathrm{T}}\mathbf{V}^{\mathrm{T}}\right)^{-1}, \tag{48}$$

where

$$\mathbf{H} = \begin{bmatrix} A_{11} & \dots & A_{M_rM_t} \\ B_{11} & \dots & B_{M_rM_t} \end{bmatrix}_{M_rM_t\times M_rM_t}, \tag{49}$$

$$\boldsymbol{\Lambda} = 8\pi^2\mathrm{SNR}\left(f_c^2+\beta^2\right)\mathbf{I}_{M_rM_t\times M_rM_t}, \tag{50}$$

$$\mathbf{H} = \frac{4\pi f_c\mathrm{SNR}}{|\zeta|^2}\begin{bmatrix} -\zeta_{im} & \zeta_{re} \\ \vdots & \vdots \\ -\zeta_{im} & \zeta_{re} \end{bmatrix}_{M_rM_t\times 2}, \tag{51}$$

and

$$\boldsymbol{\Lambda}_{\zeta} = \mathrm{SNR}\frac{M_tM_r}{|\zeta|^2}\mathbf{I}_{2\times 2}, \tag{52}$$

where $\mathrm{SNR} = \frac{E}{|\zeta|^2}$, and $\beta = \frac{\int_B f^2|S(f)|^2df}{\int_B|S(f)|^2df}$ is the effective bandwidth and the integration is over the bandwidth $B$. The elements of matrix $\mathbf{H}$ are defined as $A_{lk} = \cos\phi_{tk} + \cos\phi_{rl}$ and $B_{lk} = \sin\phi_{tk} + \sin\phi_{rl}$, where $\phi_{tk} = \tan^{-1}\left(\frac{y_t-y_{tk}}{x_t-x_{tk}}\right)$ and $\phi_{rl} = \tan^{-1}\left(\frac{y_t-y_{rl}}{x_t-x_{rl}}\right)$ are the phases that reveal the geometric relationship between the Tx-Rx locations and the target position.

The minimum mean square errors (MMSEs) in the estimate of the target's x- and y-coordinates are, respectively,

$$\sigma_x^2(\mathrm{MMSE}) = \frac{c^2}{8\pi^2SNR\left(f_c^2+\beta^2\right)\cdot\frac{e_x}{u_{CRLB}}}, \tag{53}$$

and

$$\sigma_y^2(\mathrm{MMSE}) = \frac{c^2}{8\pi^2SNR\left(f_c^2+\beta^2\right)\cdot\frac{e_y}{u_{CRLB}}}, \tag{54}$$

where the coefficients

$$e_x = \left[\sum_{l=1}^{M_r}\sum_{k=1}^{M_t}\left(B_{lk}^2 - \frac{\left(\sum_{l=1}^{M_r}\sum_{k=1}^{M_t}\left(B_{lk}^2\right)\right)^2}{\left(1+\frac{\beta^2}{f_c^2}\right)M_rM_t}\right)\right], \tag{55}$$

and

$$e_y = \left[\sum_{l=1}^{M_r}\sum_{k=1}^{M_t}\left(A_{lk}^2 - \frac{\left(\sum_{l=1}^{M_r}\sum_{k=1}^{M_t}\left(A_{lk}^2\right)\right)^2}{\left(1+\frac{\beta^2}{f_c^2}\right)M_rM_t}\right)\right]. \tag{56}$$

### D. WS-MIMO Doppler Estimation

To compute the Doppler velocities, we adopt the ML approach [10]. Define the unknown parameter vector of the $k$-th target as $\boldsymbol{\theta}^{(k)} = \left[v_x^{(k)}, v_y^{(k)}, \beta_{mn}^{(k)}\right]$, then the unknown parameter vector of all targets is denoted as $\boldsymbol{\theta} = \left[\boldsymbol{\theta}^{(1)}, \boldsymbol{\theta}^{(2)}, \dots, \boldsymbol{\theta}^{(K)}\right]$ The joint pdf of the received signal vector $\mathbf{y}_{mn} = [\mathbf{y}_{mn}^{(0)}, \mathbf{y}_{mn}^{(2)}, \dots, \mathbf{y}_{mn}^{(Q-1)}]$ is [10]

$$p(\mathbf{y}_{mn};\boldsymbol{\theta}) \propto \exp\left\{-\sum_{m=1}^{M_t}\sum_{n=1}^{M_r}\int_T\left|\sum_{k=1}^{K}y_{mn}^{(k)}(t) - \sum_{k=1}^{K}\sum_{q=0}^{Q-1}\sqrt{E}\beta_{mn}^{(k)}s_m(t-\tau_{mn}-qT_{\mathrm{PRI}})e^{j2\pi f_{mn}^{(k)}\left(v_x^{(k)},v_y^{(k)}\right)t}\right|^2dt\right\}. \tag{57}$$

Following [55], the pdf in (57) yields the ML estimation of unknown parameters as

$$\begin{aligned}\widehat{\boldsymbol{\theta}}_{ML} &= \underset{\boldsymbol{\theta}}{\mathrm{argmax}}\{\ln\, p(\mathbf{y}_{mn};\boldsymbol{\theta})\} \\ &= \underset{\boldsymbol{\theta}}{\mathrm{argmax}}\left\{-\sum_{m=1}^{M_t}\sum_{n=1}^{M_r}\int_T\left|\sum_{k=1}^{K}y_{mn}^{(k)}(t) - \sum_{k=1}^{K}\sum_{q=0}^{Q-1}\sqrt{E}\beta_{mn}^{(k)}\right.\right. \\ &\qquad \left.\left. s_m(t-\tau_{mn}-qT_{\mathrm{PRI}})e^{j2\pi f_{mn}^{(k)}\left(v_x^{(k)},v_y^{(k)}\right)t}\right|^2dt\right\}.\end{aligned} \tag{58}$$

To simplify the analysis, the complex reflectivity coefficients $\beta_{mn}^{(k)}$ are assumed to be the same for all paths under the assumption that the scatters are isotropic [10], i.e., $\beta_{mn}^{(k)} = \beta$. Then, the derivative of the log-likelihood function with respect to $\beta$ vanishes, i.e.,

$$\frac{\partial}{\partial\beta_{mn}^{(k)}}\ln\, p(\mathbf{y}_{mn};\boldsymbol{\theta}) = 0. \tag{59}$$

The ML estimate of $\beta$ becomes

$$\widehat{\beta}_{ML} = \frac{1}{\sqrt{E}\rho}\sum_{m=1}^{M_r}\sum_{n=1}^{M_t}\sum_{q=0}^{Q-1}\sum_{k=1}^{K}\int_T y_{mn}^{(k)}(t)s_m^{\dagger}(t-\tau_{mn}-qT_{\mathrm{PRI}})\, e^{-j2\pi f_{mn}^{(k)}\left(v_x^{(k)},v_y^{(k)}\right)t}dt. \tag{60}$$

where

$$\rho = \sum_{m=1}^{M_r}\sum_{n=1}^{M_t}\int_T\left|\sum_{q=0}^{Q-1}\sum_{k=1}^{K}y_{mn}^{(k)}(t)s_m^{\dagger}(t-\tau_{mn}-qT_{\mathrm{PRI}})\, e^{-j2\pi f_{mn}^{(k)}\left(v_x^{(k)},v_y^{(k)}\right)t}\right|^2dt. \tag{61}$$

Expanding the likelihood function yields

$$\begin{aligned}&\ln\, p(\mathbf{y}_{mn};\boldsymbol{\theta}) \\ &= -\sum_{m=1}^{M_r}\sum_{n=1}^{M_t}\int_T y_{mn}^2dt \\ &\quad + 2\beta\sum_{m=1}^{M_r}\sum_{n=1}^{M_t}\sum_{q=0}^{Q-1}\sum_{k=1}^{K}\int_T\sqrt{E}y_{mn}(t)s_m^{\dagger}(t-\tau_{mn}-qT_{\mathrm{PRI}})\end{aligned}$$

$$e^{-j2\pi f_{mn}^{(k)}\left(v_x^{(k)},v_y^{(k)}\right)t}dt$$
$$-\beta^2 E\sum_{m=1}^{M_r}\sum_{n=1}^{M_t}\int_T\left|\sum_{q=0}^{Q-1}\sum_{k=1}^{K}s_m(t-\tau_{mn}-qT_{\mathrm{PRI}})\right.$$
$$\left.e^{j2\pi f_{mn}^{(k)}\left(v_x^{(k)},v_y^{(k)}\right)t}\right|^2 dt. \tag{62}$$

Since the first and the last terms in (62) are both negative, maximizing the whole likelihood function is equivalent to maximizing the second term. By substituting $\beta$ with $\widehat{\beta}_{ML}$, it derives

$$\begin{aligned}\widehat{\boldsymbol{v}}_{ML}&=\underset{\boldsymbol{v}}{\operatorname{argmax}}\{\ln\, p(\mathbf{y}_{mn};\boldsymbol{v})\}\\&=\underset{v_x^{(k)},v_y^{(k)}}{\operatorname{argmax}}\left\{2\widehat{\beta}_{ML}\sum_{m=1}^{M_r}\sum_{n=1}^{M_t}\sum_{q=0}^{Q-1}\sum_{k=1}^{K}\int_T\sqrt{E}y_{mn}(t)\right.\\&\qquad\left.s_m^{\dagger}(t-\tau_{mn}-qT_{\mathrm{PRI}})e^{-j2\pi f_{mn}^{(k)}\left(v_x^{(k)},v_y^{(k)}\right)t}dt\right\}\\&=\underset{v_x^{(k)},v_y^{(k)}}{\operatorname{argmax}}\left\{\frac{1}{\rho}\left|\sum_{m=1}^{M_r}\sum_{n=1}^{M_t}\sum_{q=0}^{Q-1}\sum_{k=1}^{K}\int_T y_{mn}(t)\right.\right.\\&\qquad\left.\left.s_m^{\dagger}(t-\tau_{mn}-qT_{\mathrm{PRI}})e^{-j2\pi f_{mn}^{(k)}\left(v_x^{(k)},v_y^{(k)}\right)t}dt\right|^2\right\}.\end{aligned} \tag{63}$$

The discrete form of (63) is

$$\widehat{\boldsymbol{v}}_{ML}=\underset{v_x^{(k)},v_y^{(k)}}{\operatorname{argmax}}\left\{\frac{1}{\rho}\left|\sum_{m=1}^{M_r}\sum_{n=1}^{M_t}\sum_{q=0}^{Q-1}\sum_{k=1}^{K}\mathbf{y}_{mn}(k)\right.\right.$$
$$\left.\left.\mathbf{s}_m^{\dagger}(k,q)e^{-j2\pi f_{mn}^{(k)}\left(v_x^{(k)},v_y^{(k)}\right)qT_{PRI}}\right|^2\right\}. \tag{64}$$

The two-dimensional search is adopted to obtain the ML estimates of the target velocities.

Algorithm 1 below summarizes the estimation procedure of target parameters in MC-WS-MIMO radar.

**Algorithm 1** MC-WS-MIMO Radar Target Parameter Estimation

**Input:** Partially observed samples $\mathbf{X}_{mn}$ and set of indices of observed entries $\Omega$.

**Output:** Target location $(x, y)$ and velocity $(v_x, v_y)$.

1: Recover the full data matrix $\hat{\mathbf{Z}}_{mn}$ by solving the optimization problem of (20) using SVT algorithm.
2: Estimate the target's location, $(x, y)$, with maximum likelihood approach following equation (26).
3: Estimate the target's velocity, $(v_x, v_y)$, with maximum likelihood approach following equation (64).

## IV. Performance Analyses

To characterize the performance of MC-WS-MIMO radar, we derive the guarantees on the coherence and recoverability of the data matrix, statistical AF, and lower error bounds on parameter estimates.

### A. Coherence and Recoverability of $\mathbf{Z}_{mn}$

Recall the following useful result from [57]:

*Theorem 2 [57]: Assume $\mathbf{M}\in\mathbb{C}^{N\times N}$ be a matrix with real eigenvalues. Define*

$$\tau\triangleq\frac{\mathrm{tr}(\mathbf{M})}{N},\quad \kappa^2\triangleq\frac{\mathrm{tr}(\mathbf{M}^2)}{N}-\tau^2. \tag{65}$$

*Then, it holds that*

$$\tau-\kappa\sqrt{N-1}\le\lambda_{\min}(\mathbf{M})\le\tau-\frac{\kappa}{\sqrt{N-1}}, \tag{66}$$
$$\tau+\frac{\kappa}{\sqrt{N-1}}\le\lambda_{\max}(\mathbf{M})\le\tau+\kappa\sqrt{N-1}, \tag{67}$$

*where $\lambda_{\min}(\cdot)$ ($\lambda_{\max}(\cdot)$) is the minimum (maximum) eigenvalue of its matrix argument. Further, equality holds on the left (right) of (66) if and only if equality holds on the left (right) of (67) if and only if the $N-1$ largest (smallest) eigenvalues are equal.*

We now state our main performance guarantee for MC-WS-MIMO in the following Theorem 3.

*Theorem 3 (Coherence of matrix $\mathbf{Z}_{mn}$): Consider the widely separated MIMO radar system as presented in Section II and assume the set of target Doppler frequency $\left\{f_{mn}^{(k)}\right\}_{k\in\mathbb{N}_K^+}$ consists of almost surely distinct members. Define*

$$\beta_Q(\xi_t)\triangleq\sup_{x\in\left[\xi_t,\frac{1}{2}\right]}\frac{\sin^2(\pi Qx)}{\sin^2(\pi x)}, \tag{68}$$
$$\xi_t\triangleq\min_{(i,j)\in\mathbf{N}_K^+\times\mathbf{N}_K^+,i\neq j}g\left(T_{\mathrm{PRI}}\left|f_{mn}^{(i)}-f_{mn}^{(j)}\right|\right), \tag{69}$$

*and*

$$g(x)\triangleq\begin{cases}\lceil x\rceil-x,\ \lceil x\rceil-x\le\frac{1}{2}\\ x-\lfloor x\rfloor,\ \text{otherwise.}\end{cases} \tag{70}$$

*Consider that the transmit waveforms are unimodular following assumption* **C7** *and the waveform autocorrelation is denoted as*

$$\gamma\left(l_{ij}\right)=\sum_{k=l_{ij}+1}^{N}s_m(k)s_m^*\left(k-l_{ij}\right), \tag{71}$$

*where $l_{ij}=L_{mn}^{(i)}-L_{mn}^{(j)}$. If $K\le\frac{Q}{\sqrt{\beta_Q(\xi_t)}}$, the coherence of matrix $\mathbf{Z}_{mn}$ satisfies*

$$\mu(U)\le\frac{Q}{Q-(K-1)\sqrt{\beta_Q(\xi_t)}}, \tag{72}$$
$$\mu(V)\le\frac{N+L_{mn}^{(\max)}}{N-\sqrt{K-1}\sqrt{\sum_{j\neq i}^{K}\sum_{i=1}^{K}\left|\gamma\left(l_{ij}\right)\right|^2}}. \tag{73}$$

*The matrix $\mathbf{Z}_{mn}$ obeys the conditions* **A0** *and* **A1** *with $\mu_0\triangleq\max\{\mu(U),\mu(V)\}$, and $\mu_1\triangleq\sqrt{K}\mu_0$ with probability* 1.

*Proof:* We prove the bounds on $\mu(U)$ and $\mu(V)$ separately as follows.

*1) Bound on $\mu(U)$:* We would like to consider the case where both sets of ranges and velocities consist of distinct members. The compact SVD of $\mathbf{Z}_{mn}$ can be written as

$$\mathbf{Z}_{mn} = \mathbf{U}\Sigma\mathbf{V}^H, \tag{74}$$

where $\mathbf{U} \in \mathbb{C}^{Q\times K}, \mathbf{V} \in \mathbb{C}^{\left(N+L_{mn}^{(\max)}\right)\times K}$ such that $\mathbf{U}^H\mathbf{U} = \mathbf{I}_K, \mathbf{V}^H\mathbf{V} = \mathbf{I}_K$, and $\Sigma \in \mathbb{R}^{K\times K}$ is a diagonal matrix containing the singular values of $\mathbf{Z}_{mn}$. Consider the QR decomposition of $\mathbf{D}_{mn}$, i.e., $\mathbf{D}_{mn} = \mathbf{Q}_r\mathbf{R}_r$, where $\mathbf{Q}_r \in \mathbb{C}^{Q\times K}$ is such that $\mathbf{Q}_r^H\mathbf{Q}_r \equiv \mathbf{I}_K$ and $\mathbf{R}_r \in \mathbb{C}^{K\times K}$ is an upper triangular matrix. Similarly, consider the QR decomposition of $\Gamma_{mn}^T$, i.e., $\Gamma_{mn}^T = \mathbf{Q}_s\mathbf{R}_s$, where $\mathbf{Q}_s \in \mathbb{C}^{\left(N+L_{mn}^{(\max)}\right)\times K}$ is such that $\mathbf{Q}_s^H\mathbf{Q}_s \equiv \mathbf{I}_K$ and $\mathbf{R}_s$ is an upper triangular matrix. The matrix $\mathbf{R}_r\Lambda_{mn}\mathbf{R}_s^T \in \mathbb{C}^{K\times K}$ is rank-$K$ matrix and its SVD can be expressed as $\mathbf{R}_r\Lambda_{mn}\mathbf{R}_s^T = \mathbf{Q}_1\Delta\mathbf{Q}_2^H$. Here, $\mathbf{Q}_1 \in \mathbb{C}^{K\times K}$ is such that $\mathbf{Q}_1\mathbf{Q}_1^H = \mathbf{Q}_1^H\mathbf{Q}_1 = \mathbf{I}_K$ (the same holds for $\mathbf{Q}_2$) and $\Delta \in \mathbb{R}^{K\times K}$ is a non-zero diagonal matrix, containing the singular values of matrix $\mathbf{R}_r\Lambda_{mn}\mathbf{R}_s^T$. Thus, it holds that

$$\mathbf{Z}_{mn} = \mathbf{Q}_r\mathbf{Q}_1\Delta\mathbf{Q}_2^H\mathbf{Q}_s^T = \mathbf{Q}_r\mathbf{Q}_1\Delta\left(\mathbf{Q}_s^*\mathbf{Q}_2\right)^H, \tag{75}$$

is a valid SVD of $\mathbf{Z}_{mn}$ since $(\mathbf{Q}_r\mathbf{Q}_1)^H\mathbf{Q}_r\mathbf{Q}_1 = \mathbf{I}_K$ and $\left(\mathbf{Q}_s^*\mathbf{Q}_2\right)^H\mathbf{Q}_s^*\mathbf{Q}_2 = \mathbf{I}_K$. According to the uniqueness of singular values of a matrix, it holds that $\Sigma = \Delta, \mathbf{U} = \mathbf{Q}_r\mathbf{Q}_1$ and $\mathbf{V} = \mathbf{Q}_s^*\mathbf{Q}_2$.

Denote the $i$-th row of $\mathbf{Q}_r$ and $\mathbf{D}_{mn}$ as $\mathbf{Q}_r^{(i)}$ and $\mathbf{D}_{mn}^{(i)}$, respectively. The coherence of the row space of $\mathbf{Z}_{mn}$ is

$$\begin{aligned}\mu(U) &= \frac{Q}{K}\sup_{i\in\mathbb{N}_Q^+}\left\|\mathbf{Q}_r^{(i)}\mathbf{Q}_1\right\|_2^2 = \frac{Q}{K}\sup_{i\in\mathbb{N}_Q^+}\left\|\mathbf{Q}_r^{(i)}\right\|_2^2\\ &= \frac{Q}{K}\sup_{i\in\mathbb{N}_Q^+}\left\|\mathbf{D}_{mn}^{(i)}\mathbf{R}_r^{-1}\right\|_2^2\\ &\le \frac{Q}{K}\sup_{i\in\mathbb{N}_Q^+}\frac{\left\|\mathbf{D}_{mn}^{(i)}\right\|_2^2}{\sigma_{\min}^2(\mathbf{R}_r)},\\ &\le \frac{Q}{\sigma_{\min}^2(\mathbf{R}_r)},\end{aligned} \tag{76}$$

where

$$\begin{aligned}\sigma_{\min}^2(\mathbf{R}_r) &= \lambda_{\min}\left(\mathbf{R}_r^H\mathbf{R}_r\right) = \lambda_{\min}\left(\mathbf{R}_r^H\mathbf{Q}_r^H\mathbf{Q}_r\mathbf{R}_r\right)\\ &= \lambda_{\min}\left(\mathbf{D}_{mn}^H\mathbf{D}_{mn}\right).\end{aligned} \tag{77}$$

Here, we use the symbol $\lambda_{\min}(\cdot)$ to denote the minimal eigenvalue of a matrix. Thus,

$$\mu(U) \le \frac{Q}{\lambda_{\min}\left(\mathbf{D}_{mn}^H\mathbf{D}_{mn}\right)}. \tag{78}$$

*2) Bound on $\mu(V)$:* According to (78), we need a strict positive lower bound of $\lambda_{\min}\left(\mathbf{D}_{mn}^H\mathbf{D}_{mn}\right)$, with

$$\mathbf{D}_{mn}^H\mathbf{D}_{mn} = \begin{bmatrix} Q & \delta_{1,2} & \cdots & \delta_{1,K}\\ \delta_{1,2}^* & Q & \cdots & \delta_{2,K}\\ \vdots & \vdots & \ddots & \vdots\\ \delta_{1,K}^* & \delta_{2,K}^* & \cdots & Q\end{bmatrix}, \tag{79}$$

where

$$\delta_{i,j} = \sum_{q=1}^{Q} e^{\mathrm{j}2\pi q\left(f_{mn}^{(i)} - f_{mn}^{(j)}\right)T_{\mathrm{PRI}}}, \quad \forall(i,j) \in \mathbb{N}_K \times \mathbb{N}_K. \tag{80}$$

We apply Theorem 2 to matrix $\mathbf{M} \triangleq \mathbf{D}_{mn}^H\mathbf{D}_{mn} \in \mathbb{C}^{N\times N}$. The trace of $\mathbf{M}$ is $KQ$. Thus,

$$\tau = \frac{KQ}{K} = Q. \tag{81}$$

Since $\mathbf{M}$ is a Hermitian matrix, it is true that

$$\begin{aligned}\mathrm{tr}\left(\mathbf{M}^2\right) &= \sum_{k_1=1}^{K}\sum_{k_2=1}^{K}\left|\delta_{k_1,k_2}\right|^2\\ &= \sum_{k_1=1}^{K}\left\{Q^2 + \sum_{\substack{k_2=1\\k_2\neq k_1}}^{K}\left|\sum_{q=1}^{Q} e^{\mathrm{j}2\pi q\left(f_{mn}^{(k_1)} - f_{mn}^{(k_2)}\right)T_{\mathrm{PRI}}}\right|^2\right\}\\ &= \sum_{k_1=1}^{K}\left\{Q^2 + \sum_{\substack{k_2=1\\k_2\neq k_1}}^{K}\frac{\sin^2\left(\pi Q\left(f_{mn}^{(k_1)} - f_{mn}^{(k_2)}\right)T_{\mathrm{PRI}}\right)}{\sin^2\left(\pi\left(f_{mn}^{(k_1)} - f_{mn}^{(k_2)}\right)T_{\mathrm{PRI}}\right)}\right\}\\ &\triangleq \sum_{k_1=1}^{K}\left\{Q^2 + \sum_{\substack{k_2=1\\k_2\neq k_1}}^{K}\phi_Q^2\left(\left(f_{mn}^{(k_1)} - f_{mn}^{(k_2)}\right)T_{\mathrm{PRI}}\right)\right\},\end{aligned} \tag{82}$$

where

$$\phi_Q(x) \triangleq \frac{\sin(\pi Qx)}{\sin(\pi x)}, \ x \in \mathbb{R}, \ Q \in \mathbb{N}^+. \tag{83}$$

For $x \in \left[k, k+\frac{1}{2}\right], \forall k \in \mathbb{Z}$, the sequence of $\phi_Q^2(x)$ is strictly decreasing. Define $\xi_t \triangleq \min_{i\neq j} g\left(\left|\alpha_i^t - \alpha_j^t\right|\right) \in \left[0, \frac{1}{2}\right]$, where

$$g(x) \triangleq \begin{cases}\lceil x\rceil - x, \lceil x\rceil - x \le \frac{1}{2}\\ x - \lfloor x\rfloor, \text{otherwise.}\end{cases} \tag{84}$$

The upper bound of (82) is

$$\begin{aligned}\mathrm{tr}\left(\mathbf{M}^2\right) &= \sum_{k_1=1}^{K}\left\{Q^2 + (K-1)\sup_{x\in\left[\xi_t,\frac{1}{2}\right]}\phi_Q^2(x)\right\}\\ &\triangleq KQ^2 + K(K-1)\beta_Q(\xi_t).\end{aligned} \tag{85}$$

According to Theorem 2,

$$\lambda_{\min}(\mathbf{M}) = \lambda_{\min}\left(\mathbf{D}_{mn}^H\mathbf{D}_{mn}\right) \ge Q - (K-1)\sqrt{\beta_Q(\xi_t)}. \tag{86}$$

Therefore, if $K \le \frac{Q}{\sqrt{\beta_Q(\xi_t)}}$, it holds that

$$\mu(U) \le \frac{Q}{Q - (K-1)\sqrt{\beta_Q(\xi_t)}}. \tag{87}$$

The coherence of the column space of $\mathbf{Z}_{mn}$ is

$$\begin{aligned}\mu(V) &= \frac{N + L_{mn}^{(\max)}}{K}\sup_{i\in\mathbb{N}_{N+L_{mn}^{(\max)}}^+}\left\|\mathbf{Q}_s^{*(i)}\mathbf{Q}_2\right\|_2^2\\ &= \frac{N + L_{mn}^{(\max)}}{K}\sup_{i\in\mathbb{N}_{N+L_{mn}^{(\max)}}^+}\left\|\mathbf{Q}_s^{(i)}\right\|_2^2\\ &= \frac{N + L_{mn}^{(\max)}}{K}\sup_{i\in\mathbb{N}_{N+L_{mn}^{(\max)}}^+}\left\|\left(\Gamma_{mn}^T\right)^{(i)}\mathbf{R}_s^{-1}\right\|_2^2\\ &\le \frac{N + L_{mn}^{(\max)}}{K}\sup_{i\in\mathbb{N}_{N+L_{mn}^{(\max)}}^+}\left\|\left(\Gamma_{mn}^T\right)^{(i)}\right\|_2^2\\ &\quad\cdot\frac{1}{\sigma_{\min}^2(\mathbf{R}_s)},\end{aligned} \tag{88}$$

where

$$\sigma_{\min}^2(\mathbf{R}_s) = \lambda_{\min}\left(\mathbf{R}_s^H\mathbf{R}_s\right) = \lambda_{\min}\left(\mathbf{R}_s^H\mathbf{Q}_s^H\mathbf{Q}_s\mathbf{R}_s\right) = \lambda_{\min}\left(\left(\Gamma_{mn}^T\right)^H\Gamma_{mn}^T\right). \tag{89}$$

Define $\Phi = \left(\Gamma_{mn}^T\right)^H\Gamma_{mn}^T$. It holds that

$$\Phi = \begin{bmatrix} \gamma(0) & \gamma^*(l_{12}) & \cdots & \gamma^*(l_{1K}) \\ \gamma(l_{12}) & \gamma(0) & \cdots & \gamma^*(l_{2K}) \\ \vdots & \vdots & \ddots & \vdots \\ \gamma(l_{1K}) & \gamma(l_{2K}) & \cdots & \gamma(0) \end{bmatrix}, \tag{90}$$

where $l_{ij} = L_{mn}^{(i)} - L_{mn}^{(j)}$ and $\gamma\left(l_{ij}\right)$ is the waveform auto-correlation function, i.e.,

$$\begin{aligned}\gamma\left(l_{ij}\right) &= \mathbf{s}_m^H\left(C_{L_{mn}^{(i)}}^T\right)^H C_{L_{mn}^{(j)}}^T\mathbf{s}_m \\ &= \mathbf{s}_m^H\mathbf{J}_{l_{ij}}\mathbf{s}_m \\ &= \sum_{k=l_{ij}+1}^{N} s_m(k)s_m^*\left(k-l_{ij}\right).\end{aligned} \tag{91}$$

Here, $\mathbf{J}_n$ is a shifting matrix [46], defined as

$$\mathbf{J}_n = \begin{bmatrix} \overbrace{0\cdots0}^{n}1 & & 0 \\ & \ddots & \\ & & 1 \\ 0 & & \end{bmatrix}_{N\times N}. \tag{92}$$

Thus,

$$\tau = \frac{\mathrm{tr}(\Phi)}{K} = \gamma(0), \tag{93}$$

$$\mathrm{tr}\left(\Phi^2\right) = K\left(|\gamma(0)|^2 + \sum_{j\neq i}^{K}\sum_{i=1}^{K}\left|\gamma\left(l_{ij}\right)\right|^2\right). \tag{94}$$

Then, according to Theorem 2,

$$\lambda_{\min}(\Phi) \geq \gamma(0) - \sqrt{K-1}\sqrt{\sum_{j\neq i}^{K}\sum_{i=1}^{K}\left|\gamma\left(l_{ij}\right)\right|^2}. \tag{95}$$

For unimodular sequence, it is easy to verify that

$$\gamma(0) = N, \quad \sup_{i\in\mathbb{N}^+_{N+L_{mn}^{(\max)}}}\left\|\left(\Gamma_{mn}^T\right)^{(i)}\right\|^2 = K. \tag{96}$$

We have

$$\begin{aligned}\mu(V) &\leq \frac{N+L_{mn}^{(\max)}}{K}\frac{\sup_{i\in\mathbb{N}^+_{N+L_{mn}^{(\max)}}}\left\|\left(\Gamma_{mn}^T\right)^{(i)}\right\|^2}{\gamma(0)-\sqrt{K-1}\sqrt{\sum_{j\neq i}^{K}\sum_{i=1}^{K}\left|\gamma\left(l_{ij}\right)\right|^2}} \\ &= \frac{N+L_{mn}^{(\max)}}{N-\sqrt{K-1}\sqrt{\sum_{j\neq i}^{K}\sum_{i=1}^{K}\left|\gamma\left(l_{ij}\right)\right|^2}}.\end{aligned} \tag{97}$$

If the unimodular waveform sequences are designed to have ideal auto-correlation properties, i.e.,

$$\gamma(l) = 0, \quad l = 1,\ldots,\max_{j\neq i}\left|L_{mn}^{(i)} - L_{mn}^{(j)}\right|, \tag{98}$$

the coherence of the column space of $\mathbf{Z}_{mn}$ satisfies

$$\mu(V) \leq 1 + \frac{L_{mn}^{(\max)}}{N}. \tag{99}$$

■

*Remarks:* Theorem 4 suggests that the maximum time-difference-of-arrival, denoted as $L_{mn}^{(\max)}$, or alternatively the distribution of transmitting and receiving antennas, can influence the coherence of the radar data matrix. This implies that, given identical target locations, the recovery performance of matrix completion may vary depending on the geometry of the antenna setup.

### *B. Ambiguity Function of WS-MIMO Radar*

The ambiguity function (AF) characterizes radar's ability to distinguish two closely-spaced targets [58], [59], [60], [61]. In [59], WS-MIMO radar AF is based on the ML and Kullback-directed divergence (KDD) [60]. Alternatively, [61] proposes an AF for distributed MIMO radar while avoiding the large matrix inversions. We adopt this definition of AF to evaluate the performance of WS-MIMO radar with different antenna geometries and SNRs. Recall the received signal

$$\begin{aligned}y_{mn}(t) = \sum_{q=0}^{Q-1}&\sqrt{E}\beta_{mn}s_m(t-\tau_{mn}-qT_{\mathrm{PRI}}) \\ &\times e^{\mathrm{j}2\pi f_{mn}t}e^{-j2\pi f_c\tau_{mn}} + w_{mn}(t).\end{aligned} \tag{100}$$

To further simplify (100), define

$$\alpha_{mn}(\boldsymbol{\theta}) = \sqrt{E}\beta_{mn}e^{-j2\pi f_c\tau_{mn}},$$

and

$$\gamma_{mn}(t,\boldsymbol{\theta}) = \sum_{q=0}^{Q-1}s_m(t-\tau_{mn}-qT_{\mathrm{PRI}})e^{\mathrm{j}2\pi f_{mn}t}, \tag{101}$$

where $\boldsymbol{\theta} = \left[x, y, v_x, v_y\right]^{\mathrm{T}}$ is the vector containing target position and Doppler velocity. Then (100) becomes

$$y_{mn}(t) = \gamma_{mn}(t,\boldsymbol{\theta})\alpha_{mn}(\boldsymbol{\theta}) + w_{mn}(t). \tag{102}$$

After sampling, we rewrite the discretized (102) as a $\left(N+L_{mn}^{(\max)}\right)\times 1$ vector

$$\mathbf{y}_{n,m} = \boldsymbol{\gamma}_m(\boldsymbol{\theta},n)\alpha_{n,m}(\boldsymbol{\theta}) + \mathbf{w}_n. \tag{103}$$

Collecting the samples for all antennas, we obtain the received signal matrix

$$\mathbf{Y} = \boldsymbol{\Upsilon}(\boldsymbol{\theta})\boldsymbol{\alpha}(\boldsymbol{\theta}) + \mathbf{W}, \tag{104}$$

which turns out to be a $\left(N+L_{mn}^{(\max)}\right)M_r \times M_r$ block matrix

$$\mathbf{Y} = \begin{bmatrix} \boldsymbol{\gamma}_1 & 0 & \ldots & 0 \\ 0 & \boldsymbol{\gamma}_2 & \ldots & 0 \\ \vdots & \vdots & \ddots & \vdots \\ 0 & 0 & \ldots & \boldsymbol{\gamma}_{M_r} \end{bmatrix}, \tag{105}$$

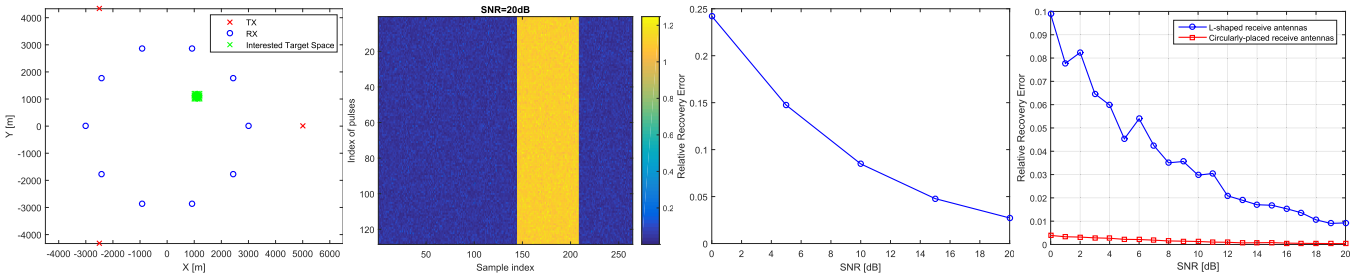


(a) (b) (c) (d)

Fig. 1. (a) An illustration of WS-MIMO radar with $M_t = 3$ transmit and $M_r = 10$ receive antennas. (b) The data matrix at receive antenna $\mathbf{p}_r = [2427.1, -1763.4]^T$ corresponding to signal from the transmitter at $\mathbf{p}_t = [-2500, -4330.1]^T$ reflected from the target located at $\mathbf{p} = [1100, 1100]^T$. (c) Matrix recovery error $\varepsilon$ as a function of SNR for the WS-MIMO configuration of Fig. 1 (a). The error is averaged over all 30 Tx-Rx pairs; (d) Matrix recovery error $\varepsilon$ as a function of SNR for the WS-MIMO configuration of Fig. 2 (a) and 2 (d) respectively. .

such that

$$\begin{aligned}\boldsymbol{\gamma}_n &= \sum_{m=1}^{M_t} \mathbf{y}_{n,m}, \ n = 1, 2, \cdots, M_r \\ &= \sum_{m=1}^{M_t} \boldsymbol{\gamma}_m(\boldsymbol{\theta}, n)\alpha_{n,m}(\boldsymbol{\theta}) + \mathbf{w}_n \\ &= \boldsymbol{\Upsilon}(\boldsymbol{\theta}, n)\boldsymbol{\alpha}(\boldsymbol{\theta}, n) + \mathbf{w}_n. \end{aligned} \tag{106}$$

where

$$\begin{aligned}&\boldsymbol{\Upsilon}(\boldsymbol{\theta}, n) \\ &= \left[\boldsymbol{\gamma}_1(\boldsymbol{\theta}, n), \boldsymbol{\gamma}_2(\boldsymbol{\theta}, n), \ldots, \boldsymbol{\gamma}_{M_t}(\boldsymbol{\theta}, n)\right] \in \mathbb{C}^{\left(N+L_{mn}^{(\max)}\right)\times M_t},\end{aligned} \tag{107}$$

$$\begin{aligned}&\boldsymbol{\alpha}(\boldsymbol{\theta}, n) \\ &= \left[\alpha_{n,1}(\boldsymbol{\theta}), \alpha_{n,2}(\boldsymbol{\theta}), \ldots, \alpha_{n,M_t}(\boldsymbol{\theta})\right]^{\mathrm{T}} \in \mathbb{C}^{M_t\times 1}.\end{aligned} \tag{108}$$

Then $\boldsymbol{\Upsilon}(\boldsymbol{\theta})$ and $\boldsymbol{\alpha}(\boldsymbol{\theta})$ in (104) are

$$\boldsymbol{\Upsilon}(\boldsymbol{\theta}) = \begin{bmatrix} \boldsymbol{\Upsilon}(\boldsymbol{\theta}, 1) & 0 & \ldots & 0 \\ 0 & \boldsymbol{\Upsilon}(\boldsymbol{\theta}, 2) & \ldots & 0 \\ \vdots & \vdots & \ddots & \vdots \\ 0 & 0 & \ldots & \boldsymbol{\Upsilon}(\boldsymbol{\theta}, M_r) \end{bmatrix}, \tag{109}$$

and

$$\boldsymbol{\alpha}(\boldsymbol{\theta}) = \begin{bmatrix} \boldsymbol{\alpha}(\boldsymbol{\theta}, 1) & 0 & \ldots & 0 \\ 0 & \boldsymbol{\alpha}(\boldsymbol{\theta}, 2) & \ldots & 0 \\ \vdots & \vdots & \ddots & \vdots \\ 0 & 0 & \ldots & \boldsymbol{\alpha}(\boldsymbol{\theta}, M_t) \end{bmatrix}. \tag{110}$$

According to [61] WS-MIMO AF is defined as

$$\mathcal{F}(\boldsymbol{\theta}_0, \boldsymbol{\theta}) = 1 - \frac{I(\boldsymbol{\theta}_0; \boldsymbol{\theta})}{\sup I(\boldsymbol{\theta}_0; \boldsymbol{\theta})}. \tag{111}$$

where

$$I(\boldsymbol{\theta}_0; \boldsymbol{\theta}) = \frac{1}{2}\left[\mathrm{tr}\left[\boldsymbol{R}_{\boldsymbol{\theta}}^{-1}\boldsymbol{R}_{\boldsymbol{\theta}} - \left(N + L_{mn}^{(\max)}\right) \times M_r\right] - \ln\left|\boldsymbol{R}_{\boldsymbol{\theta}_0}^{-1}\boldsymbol{R}_{\boldsymbol{\theta}}\right|\right] \tag{112}$$

is the KDD between two covariance matrices $\boldsymbol{R}_{\boldsymbol{\theta}_0}$ and $\boldsymbol{R}_{\boldsymbol{\theta}}$ with respect to received signal and the covariance matrix is

$$\begin{aligned}\boldsymbol{R}_{\boldsymbol{\theta}} &= E\left\{\mathbf{Y}\mathbf{Y}^H\right\} \\ &= E\left\{(\boldsymbol{\Upsilon}(\boldsymbol{\theta})\boldsymbol{\alpha}(\boldsymbol{\theta}) + \mathbf{W})(\boldsymbol{\Upsilon}(\boldsymbol{\theta})\boldsymbol{\alpha}(\boldsymbol{\theta}) + \mathbf{W})^H\right\} \\ &= \boldsymbol{\Upsilon}(\boldsymbol{\theta})E\left\{\boldsymbol{\alpha}(\boldsymbol{\theta})\boldsymbol{\alpha}(\boldsymbol{\theta})^H\right\}\boldsymbol{\Upsilon}(\boldsymbol{\theta})^H + \sigma_n^2\mathbf{I} \\ &= \boldsymbol{\Upsilon}(\boldsymbol{\theta})\boldsymbol{C}(\boldsymbol{\theta})\boldsymbol{\Upsilon}(\boldsymbol{\theta})^H + \sigma_n^2\mathbf{I}. \end{aligned} \tag{113}$$

Substituting (113) into (112) and applying the constant energy and SNR conditions [61], we obtain the AF as

$$\mathcal{F}(\boldsymbol{\theta}_0, \boldsymbol{\theta}) = \frac{1}{M_t M_r}\mathrm{tr}\left[\left|\boldsymbol{\Upsilon}(\boldsymbol{\theta}_0)\boldsymbol{\Upsilon}^{\mathrm{H}}(\boldsymbol{\theta})\right|^2\right]. \tag{114}$$

When $\theta = \theta_0$, the KDD $I(\boldsymbol{\theta}_0; \boldsymbol{\theta})$ reached its minimum and then ambiguity function $\mathcal{F}(\boldsymbol{\theta}_0, \boldsymbol{\theta})$ achieves its maximum. Unlike the AF of a monostatic radar systems [62], the WS-MIMO AF introduced in (114) includes the impact of the geometry of antenna distribution on the performance of WS-MIMO systems. This is helpful in determining an appropriate antenna configuration for real applications.

## V. Numerical Experiments

We evaluated the performance of our proposed MC-WS-MIMO radar through numerical experiments. Throughout all experiments, we employed singular value thresholding (SVT) [49] algorithm at the fusion center to recover the data matrix $\mathbf{Z}_{mn}$ corresponding to the $m$-th-Tx-and-$n$-th-Rx pair from its partial samples $\mathbf{X}_{mn}$.

### A. Reconstruction Error Under Different Antenna Geometry

We considered a WS-MIMO radar with $M_t = 3$ transmit and $M_r = 10$ receive antennas (Fig. 1 (a)) uniformly distributed over circles with radii 5000 m and 3000 m, respectively. The targets of interest are distributed in the area $\mathcal{S} = [1000, 1200] \times [1000, 1200]$ m$^2$. The transmitters emit Hadamard sequences [63] of length $N = 64$. The rows of the Hadamard matrix are mutually orthogonal to each other and can be used as Walsh codes in a MIMO radar. The carrier frequency parameters were set to $f_0 = 5$ GHz and $\Delta f = 50$ MHz. The CPI comprised of $Q = 128$ pulses with $T_{\mathrm{PRI}} = 25$ ms and $T_p = 6.4$ $\mu$s.

In the Nyquist case, the sampling frequency at the receive antennas is $f_s = 10$ MHz. In order to unambiguously sample the area $\mathcal{S}$, we choose the length of sampling window as $N + L_{\max} = 264$, where $L_{\max} = \max_{m,n}\left\{L_{mn}^{(\max)}\right\} = 200$.

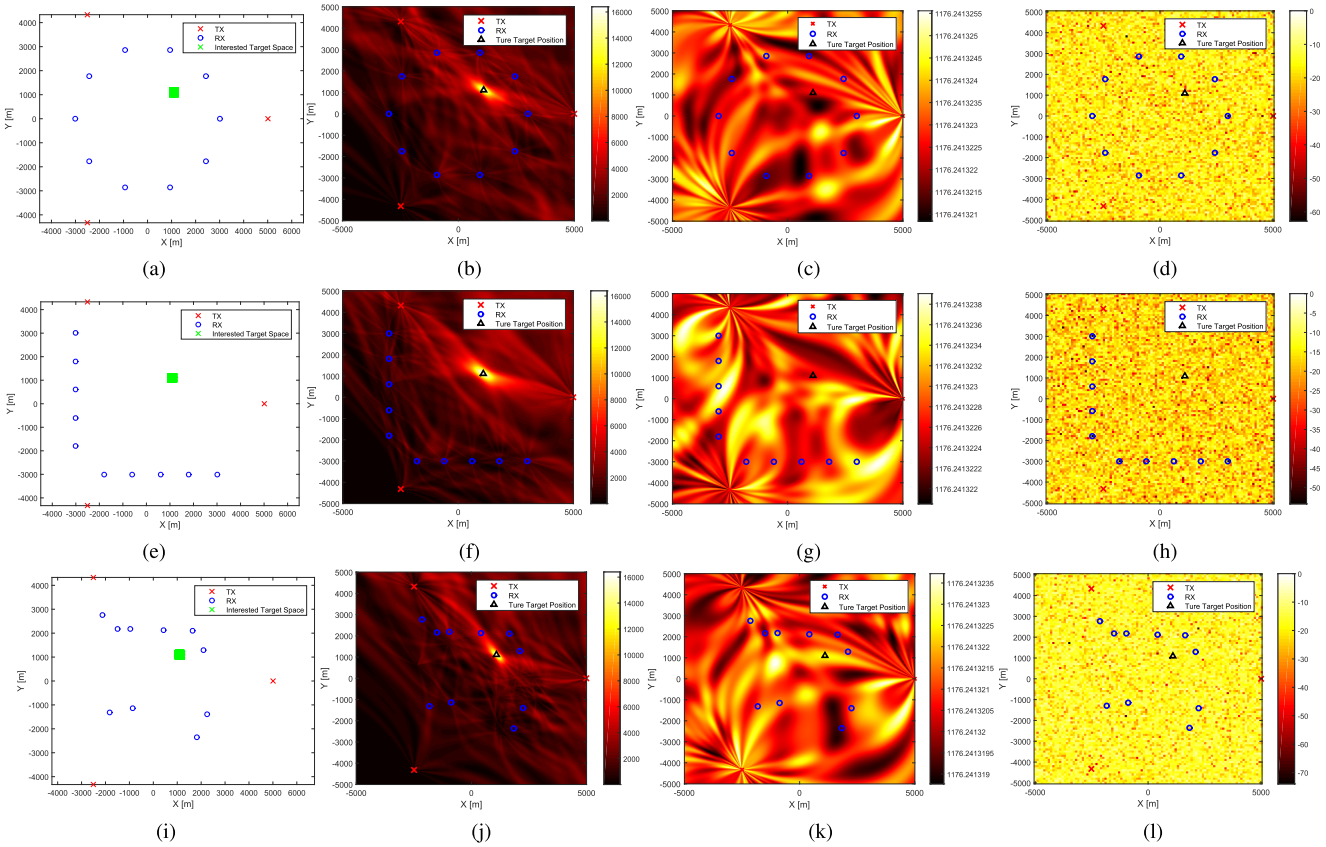


Fig. 2. The WS-MIMO radar antenna geometries and corresponding AF and PSF: (a) Circularly-placed receive antennas (b) AF corresponding to the configuration in (a) under 100% sampling rate. (c) AF corresponds to the configuration in (a) under 20% sampling rate. (d) PSF for the configuration in (a). (e-h) As in (a)-(d), respectively but for L-shaped receive antennas. (i-l) As in (a)-(d), respectively but for randomly placed receive antennas.

A single target located at $\mathbf{p} = [1100, 1100]^T$ m with velocity $\boldsymbol{v} = [10, 10]^T$ m/s is considered for recovery. Fig. 1 (b) plots the data matrix $\mathbf{Z}_{mn}$ for the receive antenna $\mathbf{p}_r = [2427.1, -1763.4]^T$ m and the reflected echo for the transmitter at $\mathbf{p}_t = [-2500, -4330.1]^T$ m at SNR = 20 dB. The noise at each receive antenna is generated independently for different Tx-Rx antenna pairs. It follows from Fig. 1 (b) that the data matrix is rank-1 and the samples of reflected echo start at range-sample index of $L_{mn}^{(1)} = 144$.

In each CPI, the $n$-th receive antenna samples only 50% of matrix $\mathbf{Z}_{mn}$, $m = 1, \cdots, M_t$ uniformly at random. At the fusion center, when these matrices are completed using SVT, we characterize the recovery performance by relative error defined as $\varepsilon = \frac{\|\mathbf{Z}_{mn} - \hat{Z}_{mn}\|_{\mathcal{F}}}{\|\mathbf{Z}_{mn}\|_{\mathcal{F}}}$, where $\hat{Z}_{mn}$ denotes the recovered matrix. For different values of SNR, Fig. 1 (c) plots the recovery error averaged over all $M_r \times M_t = 30$ Tx-Rx pairs. The error drops to approximately 3% at SNR = 20 dB. Fig. 1 (d) compares the recovery errors (averaged over 100 trials) w.r.t. two different antenna configurations. It follows that the circular antenna configuration generally exhibits an improved and robust recovery over the L-shaped geometry. Following equations (99) and (98), any change in the placement of antennas results in a corresponding change in the value of $L_{mn}^{(max)}$, which may lead to a violation of the coherence condition and a deterioration of the matrix recovery performance. In Fig. 1 (d), $L_{mn}^{(max)}$ is 200 (116) for the circularly-placed (L-shaped) antennas. Therefore, the coherence condition is not adequately satisfied for L-shaped geometry, resulting in larger relative recovery errors. The outcomes of this simulation substantiate the validity of Theorem 4.

### *B. Ambiguity Function (AF) and Point Spread Function (PSF)*

The WS-MIMO radar waveform based on Hadamard codes is used in the simulation. All plotted Ambiguity Functions (AFs) are displayed in original amplitude, without normalization or logarithmic representation. Fig. 2 shows the AF corresponding to different antenna geometry at SNR = 20 dB. In this case, we still consider WS-MIMO radar with $M_t = 3$ transmit and $M_r = 10$ receive antennas. The 3 transmit antennas are uniformly distributed over a circle with radii 5000 m as before but the 10 receive antennas distribution is changed to a circle with radii 3000 m (Fig. 2 (a)). Fig. 2 (c) displays another geometry, wherein the receive antennas are linearly spaced in an L-shape. We also consider a random geometry in Fig. 2e, wherein the receive antennas are randomly distributed over $[-3000\text{m}, 3000\text{m}] \times [-3000\text{m}, 3000\text{m}]$. From Fig. 2 (b), the AF achieves its maximum at the target's position which is consistent with the property of AF stated in Section IV-B. We observe that

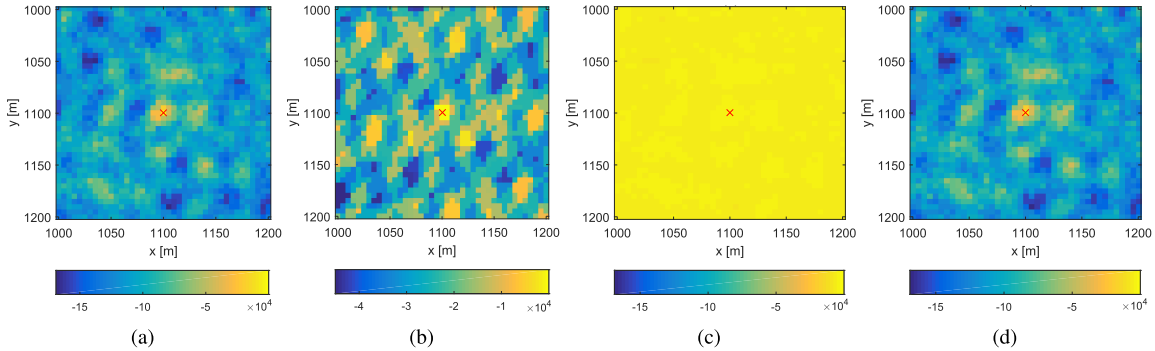


Fig. 3. The ML estimation result using subsampling and matrix recovery signals for a target at $\mathbf{p} = [1100, 1100]^T$ m with a velocity of $\boldsymbol{v} = [10, 10]^T$ m/s under the WS-MIMO radar configuration given in Fig. 1 (a), SNR = 20 dB. The red cross indicates the location of the target. (a) target localization using ML under $M_t = 3, M_r = 10$ and 50% sampling rate; (b) target localization using ML under $M_t = 2, M_r = 4$ and 50% sampling rate; (c) target localization using ML with 20% subsampled signal; (d) target localization using ML after MC-based recovery.

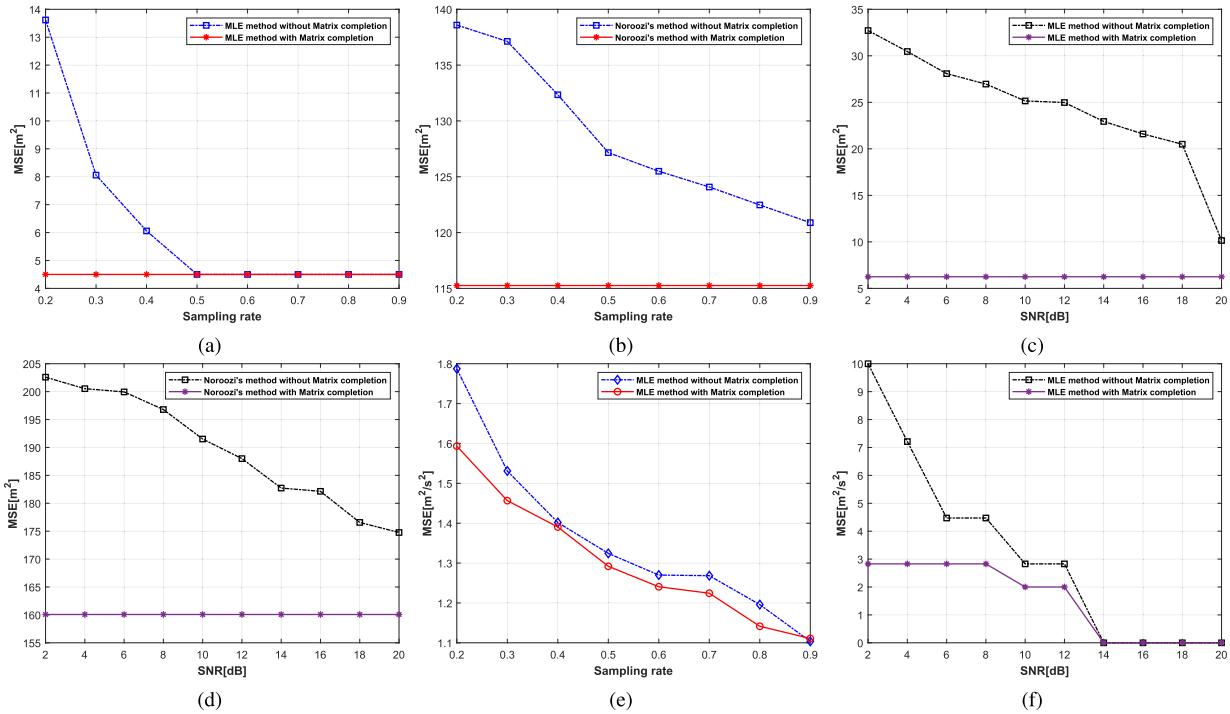


Fig. 4. Single target location and velocity estimation MSE using different methods under different sampling rates and SNRs, $M_t = 3$, $M_r = 10$. (a) Target location estimation with ML method on sub-sampled signal and MC-based recovered signal under SNR = 20dB; (b) Target location estimation with geometric method [52] on sub-sampled signal and MC-based recovered signal under SNR = 20dB; (c) Target location estimation with ML method on sub-sampled signal and MC-based recovered signal under sampling rate of 20%; (d) Target location estimation with geometric method [52] on sub-sampled signal and MC-based recovered signal under sampling rate of 20%; (e) Target velocity estimation with ML method on sub-sampled signal and MC-based recovered signal versus sampling rates; (f) Target velocity estimation with geometric method [52] on sub-sampled signal and MC-based recovered signal versus SNRs.

the AF corresponding to the L-shape linear distribution has a larger ambiguous range compared to the circular and random placement of the receive antennas. Figs. 2 (c), (f), and (i) show the AFs corresponding to different array configurations under 20% sampling rate. It follows that the AF is degenerated under a low sampling rate because stronger ambiguities appear at the positions of the transmit/receive antennas and the target. This indicates that the accuracy of localization also decreases with sub-sampling. In addition, the circularly-placed geometry has a better AF compared with the other configurations under sub-sampling.

We compared the point spread function (PSF) and ambiguity function w.r.t. the different WS-MIMO radar distributions. Following [64], [65], we employ the PSF for WS-MIMO radar. From the signal model in (12), the PSF is

$$P_{sf}\left(R_{mn}, R^*_{mn}\right) = \left|\left\langle \bar{\mathbf{z}}^{(R_{mn})}_{mn}, \mathbf{z}^{(R^*_{mn})}_{mn} \right\rangle\right| \tag{115}$$

$$= \frac{1}{M_t M_r Q} \sum_{m=1}^{M_t} \sum_{n=1}^{M_r} \mathbf{z}^{\dagger(R_{mn})}_{mn} \mathbf{z}^{(R^*_{mn})}_{mn}, \tag{116}$$

where $\mathbf{z}^{(R_{mn})}_{mn}$ is the signal waveform transmitted from the $m$-th transmit antenna to some location in the target area of interest and received by the $n$-th received antenna; and $\mathbf{z}^{(R_{mn})}_{mn}$ is the signal waveform transmitted from the $m$-th transmit antenna to the true target location and received

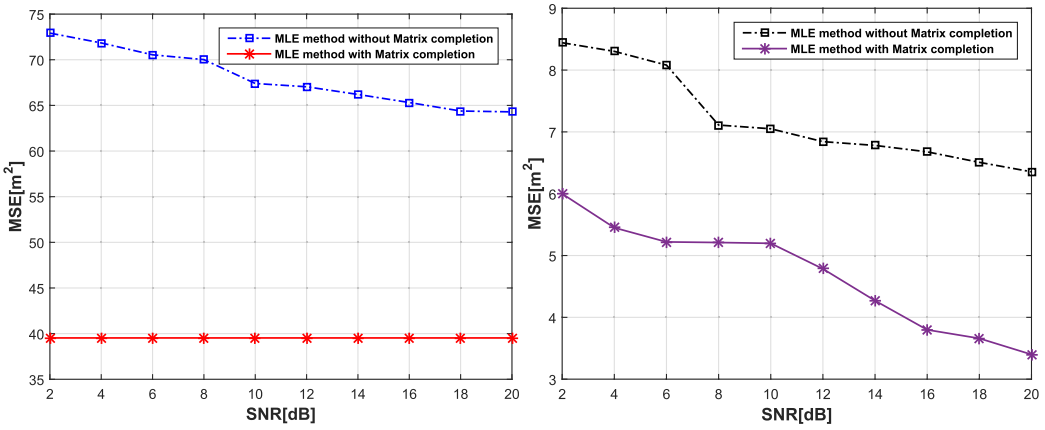


Fig. 5. Estimation MSE of (a) locations and (b) velocities using MLE under different SNRs. Here, the MSE is averaged over two targets and $M_t = 3$, $M_r = 10$.

by the $n$-th received antenna. For the WS-MIMO radar, Figs. 2 (d),(h),(l) show the PSFs in $x-y$ 2-D Cartesian coordinates on a dB scale. The PSF's peak value is at the true target location.

### C. Localization Performance Comparison

*1) Different Number of Antennas:* Fig. 3 (a) plots the ML values for the 2-D search over the area $\mathcal{S}$ for a single target at $\mathbf{p} = [1100, 1100]^T$ m with velocity $\boldsymbol{v} = [10, 10]^T$ m/s at SNR of 20 dB. Fig. 3(a) shows that the ML estimate corresponds to the true location of the target. For comparison, in Fig. 3(b), we also show the ML estimate for the same setting as in Fig. 3(a) except that the number of antennas is reduced to $M_t = 2$ and $M_r = 4$. We note the range resolution decreases with the number of transmit-receive pairs.

After reconstructing the matrices $\mathbf{Z}_{mn}$, we show the ML-based target location estimation. Fig. 3 (c) and (d) show the ML performance for WS-MIMO radar configuration with and without MC-based recovery. At SNR $=$ 20 dB and subsampling at 20% rate, when ML is applied directly on subsampled signal (Fig. 3 (c)), estimation with ML is quite inferior when compared with its application on MC-based recovery (Fig. 3 (d)) wherein the recovery error is around $\varepsilon = 4.8\%$. Fig. 3 (a-d) are displayed in the original amplitude.

*2) Comparison With Geometric Method:* Fig. 4 (a), (b) shows the mean squared errors (MSEs) of single target localization estimation with ML and geometric [52] methods while increasing samples from 20% to 90%. We compute the MSE of target location estimation as $\frac{\sum_{i=1}^{K}(\hat{\boldsymbol{p}}^{(i)}-\boldsymbol{p}^{(i)})^2}{K}$. The MSE of target velocity estimation can be calculated similarly. In the simulation, the target was set at $[1100\text{ m}, 1100\text{ m}]^T$ with velocity of $[10\text{ m/s}, 10\text{ m/s}]^T$. The antenna distribution is the same as in Fig. 1 (a). The MC performances of ML and geometric method do not change a lot with the number of samples, thereby demonstrating the robustness of MC as well as the redundancy (or low rankness) of data. A total of 1000 Monte Carlo experiments were conducted. The MSEs of the single target localization estimation with ML and geometric

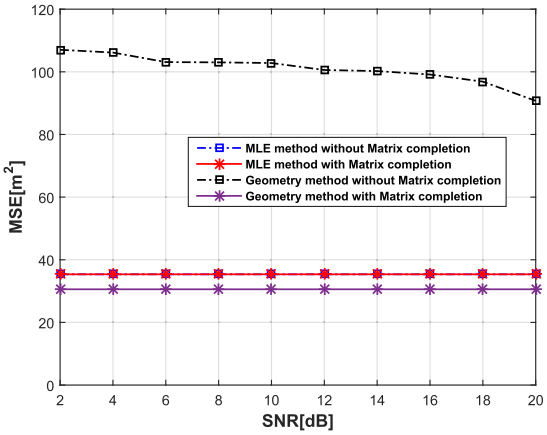


Fig. 6. The localization estimation for the single off-grid target using MLE and geometric methods under different SNRs, $M_t = 3$, $M_r = 10$.

methods versus different SNRs are shown in Fig. 4 (c), (d). The ML yields a smaller estimation MSE than the geometric method under different SNRs. Besides, the MSEs for all methods are nearly the same under different SNR values. Fig. 4 (e), (f) shows the single target velocity estimation MSE of the ML method under different sampling rates and SNRs. The velocity estimation is improved through MC when SNR is varied.

Furthermore, we also evaluated the performance for multiple target scenarios. The antenna distribution of WS-MIMO radar was the same as that in Fig. 1 (a). We considered two targets located at $[1100\text{ m}, 1100\text{ m}]^T$ and $[1200\text{ m}, 1050\text{ m}]^T$ with velocities of $[10\text{ m/s}, 10\text{ m/s}]^T$ and $[20\text{ m/s}, 20\text{ m/s}]^T$, respectively. For $1,000$ Monte Carlo simulation trials, the MSEs of target position and velocity estimates with ML methods are shown in Fig. 5 (a), (b) for different SNRs. The MSEs were calculated as the average of the MSE of each target. It follows that, after matrix completion on received data, the accuracy of both localization and velocity estimation for multiple targets is improved with ML method.

To verify that the matrix completion method for WS-MIMO radar estimation is still valid for off-grid targets,

we conducted numerical experiments in a single off-grid target scenario, where the target location is $[1025\text{ m}, 1175\text{ m}]^T$. The area of interest is the same as in previous experiments, i.e., $\mathcal{S} = [1000, 1200] \times [1000, 1200]$ m$^2$ and the grid size for ML grid-searching is 50 m. Thus, the target is off-grid, which means that ML estimates will always have bias. The geometric method, which doesn't require grid searching, has lower MSE after MC for localization estimation compared to the ML method, as shown in Fig. 6. For off-grid target location estimation, when the search grid is large, ML method does not provide better estimates after MC.

## VI. Summary

We proposed the MC-WS-MIMO radar with CDM to detect spatially diverse targets. We showed that the received signal for each Tx-Rx pair over a CPI can be modeled as a low-rank data matrix. Reduced rate sampling of the signal at each receiver results in this matrix becoming partially observed. We retrieve its missing entries using MC methods. Despite sampling at low rates, our method retrieved the unknown off-grid target parameters. Our experiments indicate target parameter recovery with an accuracy of approximately 95% at 20 dB SNR when the sampling rate is reduced to 20%. Our MC-based recovery is beneficial in enhancing the accuracy and robustness of target localization and velocity estimation in SNR-deficient scenarios. We show that further improvement in MC-based recovery is possible by analyzing the AFs for different antenna placements. This is meaningful for radar engineers in practical system design.

## References


[1] S. Sun, K. V. Mishra, and A. P. Petropulu, "Target estimation by exploiting low rank structure in widely separated MIMO radar," in *Proc. IEEE Radar Conf. (RadarConf)*, Apr. 2019, pp. 1–6.

[2] E. Fishler, A. Haimovich, R. Blum, D. Chizhik, L. Cimini, and R. Valenzuela, "MIMO radar: An idea whose time has come," in *Proc. IEEE Radar Conf.*, Apr. 2004, pp. 71–78.

[3] J. Li and P. Stoica, "MIMO radar with colocated antennas," *IEEE Signal Process. Mag.*, vol. 24, no. 5, pp. 106–114, Sep. 2007.

[4] I. Bekkerman and J. Tabrikian, "Target detection and localization using MIMO radars and sonars," *IEEE Trans. Signal Process.*, vol. 54, no. 10, pp. 3873–3883, Oct. 2006.

[5] W. Khan, I. Mansoor Qureshi, and K. Sultan, "Ambiguity function of phased-MIMO radar with colocated antennas and its properties," *IEEE Geosci. Remote Sens. Lett.*, vol. 11, no. 7, pp. 1220–1224, Jul. 2014.

[6] H. Godrich, A. M. Haimovich, and R. S. Blum, "Target localization accuracy gain in MIMO radar-based systems," *IEEE Trans. Inf. Theory*, vol. 56, no. 6, pp. 2783–2803, Jun. 2010.

[7] R. Boyer, "Performance bounds and angular resolution limit for the moving colocated MIMO radar," *IEEE Trans. Signal Process.*, vol. 59, no. 4, pp. 1539–1552, Apr. 2011.

[8] A. Haimovich, R. Blum, and L. Cimini, "MIMO radar with widely separated antennas," *IEEE Signal Process. Mag.*, vol. 25, no. 1, pp. 116–129, Dec. 2008.

[9] M. Dianat, M. R. Taban, J. Dianat, and V. Sedighi, "Target localization using least squares estimation for MIMO radars with widely separated antennas," *IEEE Trans. Aerosp. Electron. Syst.*, vol. 49, no. 4, pp. 2730–2741, Oct. 2013.

[10] Q. He, R. S. Blum, H. Godrich, and A. M. Haimovich, "Target velocity estimation and antenna placement for MIMO radar with widely separated antennas," *IEEE J. Sel. Topics Signal Process.*, vol. 4, no. 1, pp. 79–100, Feb. 2010.

[11] E. Fishler, A. Haimovich, R. S. Blum, L. J. Cimini, D. Chizhik, and R. A. Valenzuela, "Spatial diversity in radars—Models and detection performance," *IEEE Trans. Signal Process.*, vol. 54, no. 3, pp. 823–838, Mar. 2006.

[12] T. Aittomaki and V. Koivunen, "Performance of MIMO radar with angular diversity under swerling scattering models," *IEEE J. Sel. Topics Signal Process.*, vol. 4, no. 1, pp. 101–114, Feb. 2010.

[13] P. Stoica, J. Li, and Y. Xie, "On probing signal design for MIMO radar," *IEEE Trans. Signal Process.*, vol. 55, no. 8, pp. 4151–4161, Aug. 2007.

[14] M. Nazari Majd, M. Radmard, M. M. Chitgarha, A. Farina, M. H. Bastani, and M. M. Nayebi, "Spatial multiplexing gain in MIMO radars with widely separated antennas," *IET Signal Process.*, vol. 12, no. 2, pp. 207–213, Apr. 2018.

[15] H. Griffiths, "Multistatic, MIMO and networked radar: The future of radar sensors?" in *Proc. 7th Eur. Radar Conf.*, Sep. 2010, pp. 81–84.

[16] A. V. Mrstik, "Multistatic-radar binomial detection," *IEEE Trans. Aerosp. Electron. Syst.*, vol. AES-14, no. 1, pp. 103–108, Jan. 1978.

[17] E. Brookner, "MIMO radar demystified and where it makes sense to use," in *Proc. IEEE Int. Conf. Acoust., Speech Signal Process. (ICASSP)*, May 2014, pp. 5292–5296.

[18] H. Godrich, A. P. Petropulu, and H. V. Poor, "Power allocation strategies for target localization in distributed multiple-radar architectures," *IEEE Trans. Signal Process.*, vol. 59, no. 7, pp. 3226–3240, Jul. 2011.

[19] K. V. Mishra and Y. C. Eldar, "Sub-Nyquist radar: Principles and prototypes," in *Compressed Sensing in Radar Signal Processing*, A. D. Maio, Y. C. Eldar, and A. Haimovich, Eds. Cambridge, U.K.: Cambridge Univ. Press, 2019, pp. 1–48.

[20] R. Baraniuk, "Compressive sensing [lecture notes]," *IEEE Signal Process. Mag.*, vol. 24, no. 4, pp. 118–121, Jul. 2007.

[21] T. Strohmer and B. Friedlander, "Analysis of sparse MIMO radar," *Appl. Comput. Harmon. Anal.*, vol. 37, no. 3, pp. 361–388, Nov. 2014.

[22] Y. Yu, A. P. Petropulu, and H. V. Poor, "Measurement matrix design for compressive sensing–based MIMO radar," *IEEE Trans. Signal Process.*, vol. 59, no. 11, pp. 5338–5352, Nov. 2011.

[23] Y. Yu, A. P. Petropulu, and H. V. Poor, "CSSF MIMO RADAR: Compressive-sensing and step-frequency based MIMO radar," *IEEE Trans. Aerosp. Electron. Syst.*, vol. 48, no. 2, pp. 1490–1504, Apr. 2012.

[24] A. P. Petropulu, Y. Yu, and H. V. Poor, "Distributed MIMO radar using compressive sampling," in *Proc. 42nd Asilomar Conf. Signals, Syst. Comput.*, Oct. 2008, pp. 203–207.

[25] S. Gogineni and A. Nehorai, "Target estimation using sparse modeling for distributed MIMO radar," *IEEE Trans. Signal Process.*, vol. 59, no. 11, pp. 5315–5325, Nov. 2011.

[26] A. P. Petropulu, Y. Yu, and J. Huang, "On exploring sparsity in widely separated MIMO radar," in *Proc. Asilomar Conf. Signals, Syst. Comput.*, 2011, pp. 1496–1500.

[27] B. Li and A. Petropulu, "Efficient target estimation in distributed MIMO radar via the ADMM," in *Proc. 48th Annu. Conf. Inf. Sci. Syst. (CISS)*, Mar. 2014, pp. 1–5.

[28] B. Li and A. Petropulu, "Performance guarantees for distributed MIMO radar based on sparse sensing," in *Proc. IEEE Radar Conf.*, May 2014, pp. 1369–1372.

[29] Y. Yu and A. P. Petropulu, "A study on power allocation for widely separated CS-based MIMO radar," *Proc. SPIE*, vol. 8365, Jun. 2012, Art. no. 83650S.

[30] Y. Yu, S. Sun, R. N. Madan, and A. Petropulu, "Power allocation and waveform design for the compressive sensing based MIMO radar," *IEEE Trans. Aerosp. Electron. Syst.*, vol. 50, no. 2, pp. 898–909, Apr. 2014.

[31] S. Wang, Q. He, and Z. He, "Compressed sensing moving target detection for MIMO radar with widely spaced antennas," in *Proc. Int. Symp. Intell. Signal Process. Commun. Syst.*, Dec. 2010, pp. 1–4.

[32] H. Raja, W. U. Bajwa, F. Ahmad, and M. G. Amin, "Parametric dictionary learning for TWRI using distributed particle swarm optimization," in *Proc. IEEE Radar Conf. (RadarConf)*, May 2016, pp. 1–5.

[33] H. Raja, W. U. Bajwa, and F. Ahmad, "Through-the-wall radar imaging using a distributed quasi-Newton method," in *Proc. 51st Asilomar Conf. Signals, Syst., Comput.*, Oct. 2017, pp. 85–89.

[34] Y. Chi, L. L. Scharf, A. Pezeshki, and A. R. Calderbank, "Sensitivity to basis mismatch in compressed sensing," *IEEE Trans. Signal Process.*, vol. 59, no. 5, pp. 2182–2195, May 2011.

[35] R. Heckel, V. I. Morgenshtern, and M. Soltanolkotabi, "Super-resolution radar," *Inf. Inference J. IMA*, vol. 5, no. 1, pp. 22–75, 2016.

[36] K. V. Mishra, M. Cho, A. Kruger, and W. Xu, "Spectral super-resolution with prior knowledge," *IEEE Trans. Signal Process.*, vol. 63, no. 20, pp. 5342–5357, Oct. 2015.
[37] E. J. Candès and B. Recht, "Exact matrix completion via convex optimization," *Found. Comput. Math.*, vol. 9, no. 6, pp. 717–772, Dec. 2009.
[38] E. J. Candes and Y. Plan, "Matrix completion with noise," *Proc. IEEE*, vol. 98, no. 6, pp. 925–936, Jun. 2010.
[39] E. J. Candes and T. Tao, "The power of convex relaxation: Near-optimal matrix completion," *IEEE Trans. Inf. Theory*, vol. 56, no. 5, pp. 2053–2080, May 2010.
[40] K. V. Mishra, A. Kruger, and W. F. Krajewski, "Compressed sensing applied to weather radar," in *Proc. IEEE Geosci. Remote Sens. Symp.*, Jul. 2014, pp. 1832–1835.
[41] S. Sun, A. P. Petropulu, and W. U. Bajwa, "Target estimation in colocated MIMO radar via matrix completion," in *Proc. IEEE Int. Conf. Acoust., Speech Signal Process.*, May 2013, pp. 4144–4148.
[42] S. Sun, W. U. Bajwa, and A. P. Petropulu, "MIMO-MC radar: A MIMO radar approach based on matrix completion," *IEEE Trans. Aerosp. Electron. Syst.*, vol. 51, no. 3, pp. 1839–1852, Jul. 2015.
[43] D. S. Kalogerias and A. P. Petropulu, "Matrix completion in colocated MIMO radar: Recoverability, bounds & theoretical guarantees," *IEEE Trans. Signal Process.*, vol. 62, no. 2, pp. 309–321, Jan. 2014.
[44] S. Sun and A. P. Petropulu, "Waveform design for MIMO radars with matrix completion," *IEEE J. Sel. Topics Signal Process.*, vol. 9, no. 8, pp. 1400–1414, Dec. 2015.
[45] H. Sun, F. Brigui, and M. Lesturgie, "Analysis and comparison of MIMO radar waveforms," in *Proc. Int. Radar Conf.*, Oct. 2014, pp. 1–6.
[46] H. He, P. Stoica, and J. Li, "Designing unimodular sequence sets with good correlations—Including an application to MIMO radar," *IEEE Trans. Signal Process.*, vol. 57, no. 11, pp. 4391–4405, Nov. 2009.
[47] M. I. Skolnik, *Radar Handbook*, 3rd ed. New York, NY, USA: McGraw-Hill, 2008.
[48] Q. He, N. H. Lehmann, R. S. Blum, and A. M. Haimovich, "MIMO radar moving target detection in homogeneous clutter," *IEEE Trans. Aerosp. Electron. Syst.*, vol. 46, no. 3, pp. 1290–1301, Jul. 2010.
[49] J.-F. Cai, E. J. Candès, and Z. Shen, "A singular value thresholding algorithm for matrix completion," *SIAM J. Optim.*, vol. 20, no. 4, pp. 1956–1982, 2010.
[50] Q. He, R. S. Blum, and A. M. Haimovich, "Noncoherent MIMO radar for location and velocity estimation: More antennas means better performance," *IEEE Trans. Signal Process.*, vol. 58, no. 7, pp. 3661–3680, Jul. 2010.
[51] A. Hassanien, S. A. Vorobyov, and A. B. Gershman, "Moving target parameters estimation in noncoherent MIMO radar systems," *IEEE Trans. Signal Process.*, vol. 60, no. 5, pp. 2354–2361, May 2012.
[52] A. Noroozi and M. A. Sebt, "Target localization from bistatic range measurements in multi-transmitter multi-receiver passive radar," *IEEE Signal Process. Lett.*, vol. 22, no. 12, pp. 2445–2449, Dec. 2015.
[53] C.-H. Park and J.-H. Chang, "Closed-form localization for distributed MIMO radar systems using time delay measurements," *IEEE Trans. Wireless Commun.*, vol. 15, no. 2, pp. 1480–1490, Feb. 2016.
[54] A. Tajer, G. H. Jajamovich, X. Wang, and G. V. Moustakides, "Optimal joint target detection and parameter estimation by MIMO radar," *IEEE J. Sel. Topics Signal Process.*, vol. 4, no. 1, pp. 127–145, Feb. 2010.
[55] S. M. Kay, *Fundamentals of Statistical Signal Processing, Volume I: Estimation Theory*. Upper Saddle River, NJ, USA: Prentice-Hall, 1993.
[56] G. H. Golub and C. F. Van Loan, *Matrix Computations*. Baltimore, MD, USA: JHU Press, 2013.
[57] H. Wolkowicz and G. P. H. Styan, "Bounds for eigenvalues using traces," *Linear Algebra its Appl.*, vol. 29, pp. 471–506, Feb. 1980.
[58] S. Pinilla, K. Vijay Mishra, B. M. Sadler, and H. Arguello, "Phase retrieval for radar waveform design," 2022, *arXiv:2201.11384*.
[59] M. Radmard, M. M. Chitgarha, M. Nazari Majd, and M. M. Nayebi, "Ambiguity function of MIMO radar with widely separated antennas," in *Proc. 15th Int. Radar Symp. (IRS)*, Jun. 2014, pp. 1–5.
[60] M.-J. D. Rendas and J. M. Moura, "Ambiguity in radar and sonar," *IEEE Trans. Signal Process.*, vol. 46, no. 2, pp. 294–305, Feb. 1998.
[61] C. V. Ilioudis, C. Clemente, I. Proudler, and J. Soraghan, "Ambiguity function for distributed MIMO radar systems," in *Proc. IEEE Radar Conf. (RadarConf)*, May 2016, pp. 1–6.
[62] N. Levanon and E. Mozeson, *Radar Signals*. Hoboken, NJ, USA: Wiley, 2004.
[63] J. G. Proakis, *Digital Communications*, 4th ed. New York, NY, USA: McGraw-Hill, 2001.
[64] F. Liu, M. Antoniou, Z. Zeng, and M. Cherniakov, "Point spread function analysis for BSAR with GNSS transmitters and long dwell times: Theory and experimental confirmation," *IEEE Geosci. Remote Sens. Lett.*, vol. 10, no. 4, pp. 781–785, Jul. 2013.
[65] L. Ding, C. Liu, and W. Chen, "Analyzing the FD-MIMO sparse imaging under carrier frequency offsets from the perspective of point spread function," in *Proc. Asilomar Conf. Signals, Syst. Comput.*, Nov. 2013, pp. 200–204.

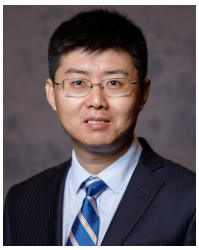

**Shunqiao Sun** (Senior Member, IEEE) received the Ph.D. degree in electrical and computer engineering from Rutgers, The State University of New Jersey, New Brunswick, NJ, USA, in January 2016. From 2016 to 2019, he was with the Radar Core Team of Aptiv, Technical Center Malibu, CA, USA, where he has worked on advanced radar signal processing and machine learning algorithms for self-driving vehicles and lead the development of direction-of-arrival estimation techniques for next-generation short-range radar sensor which has been used in over 120-million automotive radar units. In August 2019, he joined the Department of Electrical and Computer Engineering, The University of Alabama, Tuscaloosa, AL, USA, as a tenure-track Assistant Professor. He has authored a paper that won the Best Student Paper Award at 2020 IEEE Sensor Array and Multichannel Signal Processing Workshop (SAM). His research interests lie at the interface of statistical and sparse signal processing with mathematical optimizations, automotive radar, MIMO radar, machine learning, and smart sensing for autonomous vehicles.

He received the 2016 IEEE Aerospace and Electronics Systems Society (AESS) Robert T. Hill Best Dissertation Award for his thesis "MIMO radar with Sparse Sensing." He received the 2022 U.S. National Science Foundation (NSF) Computer and Information Science and Engineering (CISE) Research Initiation Initiative (CRII) Award. He was an elected member of IEEE Sensor Array and Multichannel (SAM) Technical Committee (2024–2026). He is the Vice Chair of IEEE Signal Processing Society (SPS) Autonomous Systems Initiative (ASI) Steering Committee (2023–2024). He has co-organized the First and Second Workshop on Signal Processing for Autonomous Systems (SPAS) at International Conference on Acoustics, Speech, and Signal Processing (ICASSP) 2023 in Rhodes, Greece, and ICASSP 2024 in Seoul, South Korea, respectively. He has co-organized a dozen special sessions on automotive radar signal processing, machine learning, and sparse arrays at IEEE SPS and AESS flagship conferences. He is an Associate Editor of IEEE SIGNAL PROCESSING LETTERS and IEEE OPEN JOURNAL OF SIGNAL PROCESSING.

**Yunqiao Hu** (Student Member, IEEE) received the B.S. degree in electrical engineering from Dalian Maritime University, Dalian, China, in 2019, and the M.S. degree in electrical engineering from the University of Electronic Science and Technology of China, Chengdu, China, in 2022. He is currently pursuing the Ph.D. degree in automotive radar signal processing with the Department of Electrical and Computer Engineering, The University of Alabama, Tuscaloosa, AL, USA. His research interests include automotive radar, array signal processing, multiple-input multiple-output radar with sparse sensing, and machine learning.

**Kumar Vijay Mishra** (Senior Member, IEEE) received the B.Tech. degree (summa cum laude) in electronics and communication engineering from the National Institute of Technology, Hamirpur (NITH), India, in 2003, the M.S. degree in electrical engineering from Colorado State University in 2012, and the M.S. degree in mathematics and the Ph.D. degree in electrical engineering from The University of Iowa in 2015.

He is currently working on NASA's Global Precipitation Mission Ground Validation (GPM-GV) Weather Radars. He is also a Senior Fellow with the United States DEVCOM Army Research Laboratory; a Technical Adviser to Singapore-based automotive radar start-up Hertzwell and Boston-based imaging radar startup Aura Intelligent Systems; and a Honorary Research Fellow with the SnT—Interdisciplinary Centre for Security, Reliability and Trust, University of Luxembourg. Previously, he had research appointments with the Electronics and Radar Development Establishment (LRDE), Defence Research and Development Organisation (DRDO) Bengaluru; IIHR—Hydroscience & Engineering, Iowa City, IA, USA; Mitsubishi Electric Research Laboratories, Cambridge, MA, USA; Qualcomm, San Jose; and Technion—Israel Institute of Technology. His research interests include radar systems, signal processing, remote sensing, and electromagnetics.

Dr. Mishra is a Distinguished Lecturer of the IEEE Communications Society (2023–2024), IEEE Aerospace and Electronic Systems Society (AESS) (2023–2024), IEEE Vehicular Technology Society (2023–2024), IEEE Geoscience and Remote Sensing Society (2024–2025), and IEEE Future Networks Initiative (2022). He was a recipient of the IET Premium Best Paper Prize (2021), IEEE TRANSACTIONS ON AEROSPACE AND ELECTRONIC SYSTEMS Outstanding Editor (2021), U.S. National Academies Harry Diamond Distinguished Fellowship (2018–2021), American Geophysical Union Editors' Citation for Excellence (2019), Royal Meteorological Society Quarterly Journal Editor's Prize (2017), Viterbi Post-Doctoral Fellowship (2015 and 2016), Lady Davis Post-Doctoral Fellowship (2017), DRDO LRDE Scientist of the Year Award (2006), NITH Director's Gold Medal (2003), and NITH Best Student Award (2003). He has received Best Paper Awards at IEEE MLSP 2019 and IEEE ACES Symposium 2019. Since 2021, he has been the Vice-Chair of the IEEE Synthetic Aperture Standards Committee, which is the first SPS standards committee. Since 2023, he has also been the Chair of the Synthetic Apertures Technical Working Group of the IEEE Signal Processing Society (SPS). He is the Chair (2023–2026) of the International Union of Radio Science (URSI) Commission C. He has been an elected member of three technical committees of IEEE SPS: SPCOM, SAM, and ASPS, and IEEE AESS Radar Systems Panel. He has been an Associate Editor of IEEE TRANSACTIONS ON AEROSPACE AND ELECTRONIC SYSTEMS since 2020 and IEEE TRANSACTIONS ON ANTENNAS AND PROPAGATION since 2023. He has been a Lead/Guest Editor of several special issues in journals, such as *IEEE Signal Processing Magazine*, IEEE JOURNAL OF SELECTED TOPICS IN SIGNAL PROCESSING, IEEE JOURNAL ON SELECTED AREAS IN COMMUNICATIONS, and IEEE JOURNAL OF SELECTED TOPICS IN APPLIED EARTH OBSERVATIONS AND REMOTE SENSING. He is a Lead Co-Editor of three books *Radar: Signal Processing for Joint Radar-Communications* (Wiley-IEEE Press), *Next-Generation Cognitive Radar Systems* (IET Press Radar, Electromagnetics & Signal Processing Technologies Series), and *Advances in Weather Radar* Volumes 1, 2, and 3 (IET Press Radar, Electromagnetics & Signal Processing Technologies Series).

**Athina P. Petropulu** (Fellow, IEEE) is currently a Distinguished Professor with the Electrical and Computer Engineering (ECE) Department, Rutgers, having worked as the Chair of the Department from 2010 to 2016. Prior to joining Rutgers, she was a Professor in ECE with Drexel University (1992–2010). She held visiting scholar appointments with SUPELEC, Universitè Paris Sud, Princeton University, and University of Southern California. Her research interests span the area of statistical signal processing, wireless communications, signal processing in networking, physical layer security, and radar signal processing. Her research has been funded by various government industry sponsors, including the National Science Foundation (NSF), the Office of Naval research, the U.S. Army, the National Institute of Health, the Whitaker Foundation, Lockheed Martin, and Raytheon.

She is a fellow of the American Association for the Advancement of Science (AAAS) and was a recipient of the 1995 Presidential Faculty Fellow Award given by the U.S. National Science Foundation and the White House. She has played key roles in her professional society, namely, she was the (2022–2023) President of the IEEE Signal Processing Society and the Editor-in-Chief of IEEE TRANSACTIONS ON SIGNAL PROCESSING (2009–2011) and IEEE Signal Processing Society Vice President-Conferences (2006–2008). She was the Technical Program Co-Chair of the 2023 IEEE International Conference on Acoustics Speech and Signal Processing (ICASSP), the General Co-Chair of the 2018 IEEE International Workshop on Signal Processing Advances in Wireless Communications (SPAWC), and the General Chair of the 2005 ICASSP. She was a Distinguished Lecturer of the Signal Processing Society and the IEEE Aerospace and Electronics Systems Society. For her service, she has received the 2012 IEEE Signal Processing Society Meritorious Service Award. She was also co-recipient of the 2005 *IEEE Signal Processing Magazine* Best Paper Award, the 2020 IEEE Signal Processing Society Young Author Best Paper Award (B. Li), the 2021 IEEE Signal Processing Society Young Author Best Paper Award (F. Liu), the 2021 Barry Carlton Best Paper Award by IEEE Aerospace and Electronic Systems Society, the 2022 IEEE Sensor Array and Multichannel Signal Processing Workshop Best Student Paper Award (Y. Li), the 2023 IEEE Machine Learning in Signal Processing Workshop Best Student Paper Award (S. Evmorfos), and the 2023 Stephen O. Rice Prize Best Paper Award by the IEEE Communications Society.